

Article

Pressure Evolution Mechanism of Marine Shale Reservoirs and Shale Gas Accumulation Model: Evidence from Fluid Inclusions in the Wufeng–Longmaxi Formation in the Basin Margin Structural Transition Zone in Northern Guizhou Province, China

Xingyu Li ^{1,2,*} , Wei Du ^{3,4}, Xia Feng ^{3,4}, Fulun Shi ^{3,4}, Yi Chen ^{3,4}, Yisong Wang ^{3,4}, Zhenxue Jiang ^{1,2} and Qun Luo ^{1,2}

¹ Unconventional Natural Gas Institute, China University of Petroleum, Beijing 102249, China

² State Key Laboratory of Petroleum Resources and Prospecting, China University of Petroleum, Beijing 102249, China

³ Key Laboratory of Unconventional Natural Gas Evaluation and Development in Complex Tectonic Areas, Ministry of Natural Resources, Guiyang 550001, China

⁴ Guizhou Engineering Research Institute of Oil & Gas Exploration and Development, Department of Natural Resources of Guizhou Province, Guiyang 550001, China

* Correspondence: 2020216435@student.cup.edu.cn

Abstract: The Wufeng–Longmaxi Formation in northern Guizhou Province is the dominant shale gas exploration and development strata in China. This study investigates the Shixi and Daozhen synclines, which are located in the basin margin transition zone. This region experienced complex tectonic stages and superimposed transformations, resulting in heterogeneous preservation conditions and shale reservoir pressure evolution in different tectonic units of the Wufeng–Longmaxi Formation. Based on fluid inclusion analysis, the types of fluid inclusion and the fluid filling stages of the Wufeng–Longmaxi shale reservoir were determined by laser Raman analysis and homogenization temperature and salinity tests. It was found that the fluid inclusion density and paleopressure in each filling stage were then restored. The results confirm that: ① Both the Shixi syncline and Daozhen syncline Wufeng–Longmaxi shale reservoirs experienced two fluid filling phases, in the early Yanshanian and late Yanshanian–Himalayan, respectively. In the course of tectonic evolution, the Wufeng–Longmaxi Formation in the Shixi and Daozhen synclines experienced pressure relief to some extent during the two aforementioned key fluid charging periods but remained in overpressurized states overall; ② The Wufeng–Longmaxi Formations of the Shixi and Daozhen synclines are characterized by high-density methane inclusions; ③ Based on the differences in the structural preservation conditions, the pressure evolution mechanisms of the Wufeng–Longmaxi Formation Shales during the important tectonic evolution period in northern Guizhou Province were revealed. Furthermore, differential enrichment and accumulation models of shale gas were established and named “facing thrust structural sealing type (Shixi syncline)” and “reverse fault lateral blocking type (Daozhen syncline)”.

Keywords: marine shale reservoir; Wufeng–Longmaxi Formation; pressure evolution mechanism; structural preservation conditions; differential accumulation; enrichment mechanism and model



Citation: Li, X.; Du, W.; Feng, X.; Shi, F.; Chen, Y.; Wang, Y.; Jiang, Z.; Luo, Q. Pressure Evolution Mechanism of Marine Shale Reservoirs and Shale Gas Accumulation Model: Evidence from Fluid Inclusions in the Wufeng–Longmaxi Formation in the Basin Margin Structural Transition Zone in Northern Guizhou Province, China. *Minerals* **2023**, *13*, 241. <https://doi.org/10.3390/min13020241>

Academic Editor: Thomas Gentzis

Received: 22 November 2022

Revised: 13 January 2023

Accepted: 4 February 2023

Published: 8 February 2023



Copyright: © 2023 by the authors. Licensee MDPI, Basel, Switzerland. This article is an open access article distributed under the terms and conditions of the Creative Commons Attribution (CC BY) license (<https://creativecommons.org/licenses/by/4.0/>).

1. Introduction

In recent years, Sinopec and PetroChina have successively made important achievements in Silurian shale gas exploration in Jiaoshiba, Weiyuan, Fushun–Yongchuan and Changning–Zhaotong in the Sichuan Basin and surrounding areas [1–7]. At present, the exploration and development of marine shale gas are mainly localized on the Wufeng–Longmaxi Formation in the upper Yangtze area, because the Wufeng–Longmaxi shales in

the Sichuan Basin are mainly characterized by high organic matter content (the TOC content is 1.5%–12.5%), large thickness, high thermal maturity (the R_o content is 2.6%–3.0%), strong gas-generation yield and appropriate brittleness [8–11]. As the exploration and development of shale gas resources in China continue to advance, the exploration of normal-pressure shale gas in the southeastern Sichuan/northern Guizhou Area has gradually received increasing attention. In addition, breakthroughs in the exploration and commercial development of normal-pressure shale gas have been achieved in Daozhen, Wulong, Pengshui and other areas along the basin margin [12].

Geotectonically, northern Guizhou Province is part of the southeastern Yangtze plate, which has experienced the Xuefeng, Caledonian, Hercynian, Indosinian, Yanshan and Himalayan tectonic stages. The superposition of multiple tectonic stages led to the formation of the complex structural style observed in present-day northern Guizhou Province [13,14]. The burial history of marine shale in the lower Paleozoic marine shale, the fluid activity in the organic-rich shale of the Longmaxi Formation, the evolution of reservoir pressure and the mechanism of shale gas accumulation are the key issues in studying marine shale gas accumulation in China [15,16]. The mechanisms of shale gas accumulation, preservation or transformation in the Wufeng–Longmaxi Formation during the multistage tectonic evolution in the whole southern Sichuan Basin provide an important reference for shale gas exploration in the Sichuan Basin [17–21]. The paleo-pressure can be reconstructed via the homogenization temperature and Raman spectral characteristics of fluid inclusions [22–27]. Based on the fluid characteristics and pressure evolution, researchers have deduced the period of fluid activity in the high-yield shale gas region in the southern Sichuan by using the petrographic characteristics of inclusions, the homogenization temperature, salinity of fluid inclusions and other parameters. It has also been noted that the pressure evolution process in the tectonic stage has been restored. Finally, a shale gas accumulation model was constructed based on the superposition of multistage tectonic evolution [28]. Northern Guizhou Province is located at the edge of the Sichuan basin, which has experienced the superposition and transformation of more complex tectonic stages than the interior of the basin. Based on this information, researchers analyzed the characteristics of the shale gas storage space, preservation conditions and shale gas accumulation potential of the Longmaxi Formation in northern Guizhou Province by investigating the tectonic evolution, faulting activity, deformation characteristics, shale deposition and geochemical and reservoir characteristics [29]. In recent years, Chinese researchers have systematically analyzed and established shale gas accumulation and enrichment models of the Longmaxi and Niutitang Formations in the southern Sichuan, southeastern Chongqing and southeastern Guizhou Province [30–32]. However, unlike the overpressured shale gas reservoirs of the Wufeng–Longmaxi Formation in the Sichuan Basin, sites in the northern Guizhou Province are mostly normal-pressure shale gas reservoirs. Little research has focused on the storage space characteristics of the Wufeng–Longmaxi Formation and the pressure evolution process of the key reservoir-forming period of the target layer in the northern Guizhou Basin; thus, it is difficult to further study the mechanism of pressure evolution in the Wufeng–Longmaxi Formation in the basin margin structural transition zone. This further increases the difficulty of establishing an accumulation and enrichment model of normal-pressure shale gas in the Wufeng–Longmaxi Formation of northern Guizhou Province.

This paper takes the Wufeng–Longmaxi shale of the Shixi syncline and Daozhen syncline as its main research objects. After establishing the burial history and thermal evolution history of the basin, the key reservoir formation period of the Wufeng–Longmaxi shale reservoir in northern Guizhou Province was successfully defined after obtaining the results of the microscopic characteristics of fluid inclusions, homogenization temperature and salinity, Raman spectra and reservoir spatial characteristics. Furthermore, it was found that the corresponding pressure evolution has also been restored. In combination with the structural preservation conditions, pore structure and gas content, the pressure evolution mechanism of shale reservoirs in the Wufeng–Longmaxi Formation is discussed,

underlining the importance of the structural preservation conditions in the accumulation and enrichment of shale gas. Finally, unique accumulation and enrichment models of the Wufeng–Longmaxi normal-pressure shale gas reservoir in northern Guizhou Province were constructed and named “Facing Thrust Structural Sealing Type (Shixi syncline)” and “Reverse Fault Lateral Blocking Type (Daozhen syncline)”. The Shixi syncline is located in the syncline structure formed by the hedging of two reverse faults, while the shale gas of the Wufeng–Longmaxi Formation mostly accumulates in the footwall of the hedging structure. Due to the relatively weak transformation of structural superposition that occurred in the late stage, the greater depth of the target layer and the stronger fault sealing ability, the effect of blocking shale gas escape is better. After hydrocarbon expulsion, the source rocks migrated along the bedding fractures in the Longmaxi Formation in the form of diffusions until they were blocked by large-scale hedge faults, where the shale gas accumulated. The Daozhen syncline is a shale gas reservoir with reverse fault lateral blocking, which means that the footwall destination layer is connected with a dense hanging wall that traps the shale gas in the fault footwall. Unlike the Shixi syncline, the steeper strata in the Daozhen syncline intensified the shale gas migration. After hydrocarbon expulsion, shale gas moves outward vertically and laterally along high angle fractures and bedding fractures until it is blocked laterally by large thrust faults, where the gas is enriched in large quantities. The present researches provide a reference for the further exploration of marine shale gas reservoirs in the complex structural area of northern Guizhou Province.

2. Geological Setting

The northern Guizhou area is at the margin of the Sichuan Basin, which is located in the southwestern China. The area was one of the most gas-productive basins to develop during the western Yangtze Craton [33–37]. The northern Guizhou area includes the administrative area of Guizhou Province, which is mainly distributed in the area of the eastern Zunyi and northern Guiyang–Zhenyuan faults, with an area of approximately 4.9×10^4 km². At the same time, this area is part of the Wuling Depression structural unit [38,39]. The area contains high-quality shale series, such as the lower Silurian Longmaxi Formation, lower Cambrian Niutitang Formation and other strata. It is worth noting that the study area is located in the southeastern margin of the Sichuan Basin, and its main burial history includes early subsidence (Caledonian), late uplift (Hercynian), a long depositional period (Indosinian to Yanshanian) and a short uplift period (Himalayan). As for the tectonic evolution background, the Yangtze block experienced the Xuefeng tectonic stage in the middle of the Neo-Paleozoic, the early–middle Caledonian tectonic stage in the Cambrian–Ordovician, the late Caledonian tectonic stage in the middle and late Silurian, the Hercynian tectonic stage in the Devonian–Carboniferous, the Indosinian tectonic stage in the Triassic–Jurassic and the Cretaceous Yanshan and Himalayan tectonic stages from the Paleogene to the present. From previous research, it is clear that the northern Guizhou region is part of the Yangtze continental block in terms of its tectonic position, which means its tectonic evolution is consistent with that of the Yangtze continental block [13,40–42]. The lower Silurian Longmaxi Formation in northern Guizhou Province has experienced numerous tectonic stages, namely, the Caledonian, Hercynian, Indosinian, Yanshanian and Himalayan [43]. The study area mainly contains NE, EW and NE faults. Furthermore, the superposition and transformation of multiple tectonic stages which have cut, combined and interfered with multiple trending faults in the study area have given rise to the complex macroscopic fracture distribution characteristics that may be observed today [44]. Overall, the Shixi syncline is located in the Fenggang South–North trough fold deformational area of the northern Guizhou uplift. The faults in the west are relatively developed, with eastward dips of 15–35°, while those in the east have westward dips of 40–65°. As can be seen from the above data, the Shixi syncline has an obvious characteristic, which indicates steepness in the west and gentleness in the east, in which the direction of the tectonic line is nearly North–South. The Daozhen syncline is located in the NNE structural deformation area of the Fenggang area, which is the Zunyi fault arch of the northern Guizhou platform uplift

on the southern margin of the Yangtze platform. The fault is underdeveloped, with an axis direction of 15–20° NE in the Daozhen syncline and a wide and gentle structural shape [45].

The exposed strata in northern Guizhou Province mainly include Nanhua, Sinian, Cambrian, Ordovician, Silurian and Permian strata. The lower Silurian Longmaxi Formation was affected by the middle Guizhou paleo-uplift, resulting in partially missing and denuded strata in the southern region. In terms of sedimentary characteristics, the Longmaxi Formation in northern Guizhou Province is characterized by a shallowing upward sedimentary sequence. The mineral composition of the Wufeng–Longmaxi shale in northern Guizhou Province is mainly quartz (average content: 40%–60%). Furthermore, the formation is a deep-water shelf facies with high biogenic siliceous content, which is conducive to shale gas hydraulic fracturing, making it a sweet-spot area for shale gas enrichment and exploitation. The lithology is mainly carbonaceous mudstone and siltstone, and its lower part is a set of black carbonaceous mudstones with thicknesses from tens of meters to 100 m. Notably, the formation has abundant graptolite fossils, such as *Didymograptus McCoyi*, *Rastrites*, *Orthograptus*, and *Glyptograptus Lapworthi*, which have abundant organic matter [14]. In the Shixi syncline, carbonaceous shale, silty shale and calcareous shale are present from bottom to top in the first member of the Wufeng–Longmaxi Formation. From bottom to top, the lithology of the Longmaxi Formation in the western Daozhen syncline is mainly composed of carbonaceous mudstone, dark gray calcium-containing carbonaceous mudstone, calcareous mudstone, bioclastic limestone and gray calcium-containing calcareous mudstone. During the depositional period of the lower Silurian Longmaxi Formation in this region, the global sea level rose rapidly, and thick siliceous shale developed in and around the Sichuan Basin. As the global sea level slowly declined, the depositional environment became shallower and the supply of terrigenous clastic materials gradually increased, which led to the sediments in the study area gradually evolving into bioclastic limestone, calcareous shale and silty shale [46].

As shown in Figure 1, under the overthrust and nappe of the Jiangnan Xuefeng inland orogenic belt, the northern Guizhou region began to uplift on a large scale in the late Yanshanian. The uplifting parts then changed from southeast to northwest, with the overall uplifting time between 95–80 Ma. The Shixi 1 well is located in the east of the Zunyi–Nanchuan Fault, farthest from the Jiangnan Xuefeng orogenic belt. The uplifting time was about 80 Ma, the range was about 4450 m, and the buried depth was about 1360 m. The current pressure coefficient of the shale gas reservoir is about 1.10, and the gas content is about 4.11 m³/t, which shows the rich preservation conditions. The Daoye 1 well is located in the Daozhen syncline, closest to Jiangnan Xuefeng orogenic belt. Its uplift time was about 90 Ma earlier than that of the Shixi 1 well. In the later stage, it experienced stronger uplift and denudation in the Daozhen region, with a denudation thickness of up to 5200 m leading to a burial depth of about 600 m; the gas content is about 3.40 m³/t, which shows the poor preservation conditions. It can be seen that early escape played a key role in the destruction of shale gas reservoirs.

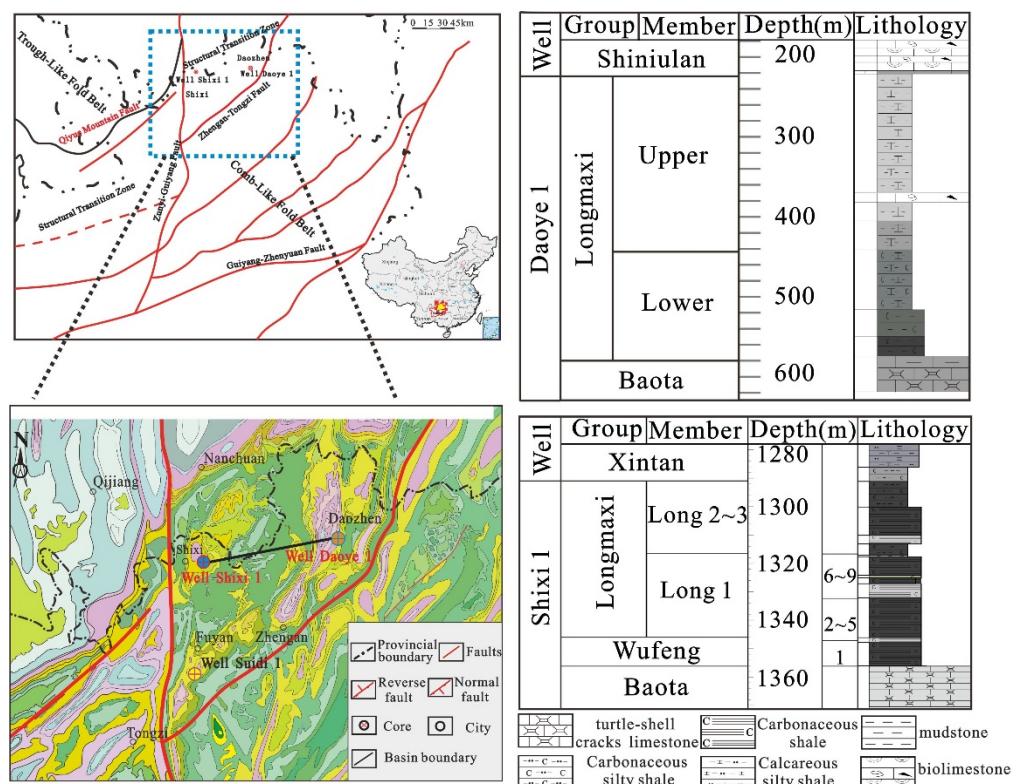


Figure 1. Structural outline map of the study area in northern Guizhou Province and comprehensive stratigraphic histogram of the Shixi 1 and Daoye 1 wells.

3. Sampling and Methodology

3.1. Samples

Fluid inclusions and laser Raman analysis samples were collected from the outcrops of the western Daozhen syncline, the western Shixi syncline and the Silurian Longmaxi Formation in the Shixi 1 well. Specifically, we selected SXX-15-8 (western Shixi syncline) as an outcrop, DZXX-1-5 (western Daozhen syncline) as an outcrop and SX-87 (Shixi 1 well) as the core as test objects. Field emission scanning electron microscopy samples were collected from the lower Silurian Longmaxi Formation in the Daoye 1 and Shixi 1 wells. The average porosities of the major shale gas-producing layers (first member of the Longmaxi Formation) in the Shixi 1 and Daoye 1 wells are 3.07% and 3.02%, respectively. The gas contents of the Shixi 1 and Daoye 1 wells are 4.11 m³/t and 3.40 m³/t, respectively. The filling of pyrite veins in the bedding are common in the target layer of the Shixi 1 well, and high-angle calcite veins are visible in the target layer of the western Shixi and Daozhen synclines.

3.2. Methodology

Temperature and salinity measurements of fluid inclusions were carried out using a ZEISS Imager M2m research grade polarized light fluorescence microscope produced by Zeiss Company in Oberkochen, Germany and equipped with a LINKAM THMS600 high-temperature table produced by Linkam Company in Lincolnshire, UK. The temperature error after correction of the hot and cold stages was ± 0.1 °C (Figure 2A). During the temperature measurements of fluid inclusions, the rate of temperature change during the hot and cold stages was controlled to within 0.1 to 5 °C/min. Then, the temperature was observed and recorded when the inclusions were completely homogeneous and the inclusion ice cubes were completely melted, and the homogenization temperatures and salinities of the hydrocarbon-containing brine inclusions coexisting with the methane inclusions were measured.

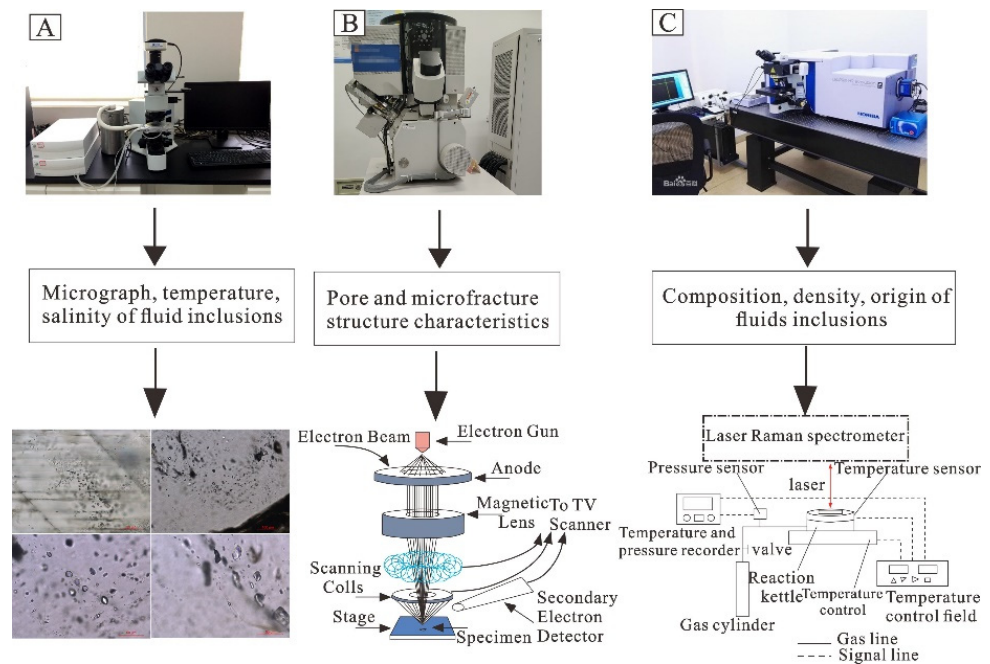


Figure 2. Experimental test flow chart. (A) LINKAM THMS600 high-temperature table; (B) FEI Helios NanoLab 650 field emission scanning electron microscope; (C) LABHR-VIS LabRAM HR800 research grade laser Raman spectrometer.

Laser Raman spectroscopic measurements were performed using a LABHR-VIS LabRAM HR800 research grade laser Raman spectrometer produced by HORIBA Jobin Yvon S.A.S in Paris, France (Figure 2C). The experimental temperature and humidity were controlled at 25 °C and 50%, respectively. A Yag laser was used for the test; the wavelength was 532 nm, the power was controlled at 20 mW, the line width was less than 1 nm and the scanning range was 100–4200 cm^{-1} . In the laser Raman spectrum data acquisition of inclusions, 300 gratings were first selected to obtain signal peaks to determine the composition of the inclusions, and then 1800 gratings were used to collect and determine the peak displacement. Finally, the measured results were corrected with the neon laser Raman standard peak Ne_1 (standard value of 2836.9888 cm^{-1}) and standard peak Ne_3 (standard value of 3008.1274 cm^{-1}) [47,48].

A FEI Helios NanoLab 650 field emission scanning electron microscope (FE-SEM) in Oberkochen, Germany was used to observe the spatial characteristics of the shale reservoirs, with a maximum resolution of 0.8 nm (Figure 2B). However, due to the poor conductivity of shale samples, the resolution was generally only approximately a few nanometers.

Based on the above methods, the main ideas of this study are as follow: Firstly, combining the distribution characteristics of filling veins in outcrop and core samples with the microscopic characteristics of fluid inclusions, the development stages of fluid inclusions were divided. Then, after obtaining the homogenization temperature and laser Raman spectra of the fluid inclusion, the trapping pressure of the inclusion was calculated. Further, the pressure coefficient of the target layer was obtained. In addition, the source of fluid inclusions could be determined by laser Raman spectroscopy and paleosalinity tests. Next, on the basis of establishing the burial and thermal evolution history of the sedimentary basins, the periods of fluid activity were defined by two-dimensional projection. Finally, this study referred to the seismic profile data of the study area. Combined with the differences in structural preservation conditions since the Himalayan period, the corresponding pressure evolution during fluid activity and the macroscopic and microscopic characteristics of fracture veins, shale gas enrichment models of the complex structural belt of northern Guizhou Province were established.

4. Results

4.1. Petrographic Characteristics

Veins in shale gas reservoirs are the products of multiphase fluid interactions under pressure control, which are often associated with fractures [49–51]. Observations of core fractures and veins reveal that most of the shale fractures in the Wufeng–Longmaxi Formation of northern Guizhou Province are filled with pyrite and calcite (Figure 3). Bedding-parallel pyrite veins and calcite veins are common in the cored section of the Shixi 1 well (Figure 3A,B), and calcite veins are visible in the western Shixi syncline (Figure 3C), the western Daozhen syncline (Figure 3D) and the Daoye 1 well (Figure 3G). In the Longmaxi Formation, some bedding fractures and high-angle fractures have developed (Figure 3E,F,H). Tests of samples using a microscope showed that gas–liquid two-phase brine inclusions and pure gas-phase methane inclusions were present in samples SXX-15-8, SX-87, and DZXX-1-5.



Figure 3. Characteristics of shale vein development in the Wufeng–Longmaxi Formation. (A) Pyrite nodules in the first member of the Longmaxi Formation in the Shixi 1 well; (B) Bedding-parallel calcite veins in the first member of the Longmaxi Formation in the Shixi 1 well; (C) Calcite veins in an outcrop in the western Shixi syncline; (D) Calcite veins in an outcrop in the western Daozhen syncline; (E) Bedding-parallel calcite veins in the second member of the Longmaxi Formation in the Shixi 1 well; (F) High angle cracks in the second member of the Longmaxi Formation in the Shixi 1 well; (G) Calcite veins of the Longmaxi Formation in the Daoye 1 well; (H) High-angle fractures of the Longmaxi Formation in the Daoye 1 well.

The Oil Fluid Inclusion Abundance Index, which means grains with oil inclusions (GOI), refers to the percentage of the framework mineral particles containing oil inclusions of the total mineral particles in a rock sample, thereby indicating the degree of oil and gas filling over the geological history of the area. Generally speaking, a GOI < 1% indicates that the formation has not experienced hydrocarbon charging history. A GOI from 1% to 5% indicates that the formation has experienced a small amount of oil and gas charging, and GOI > 5% indicates that the formation has experienced large-scale oil and gas charging. Gas inclusions in fractured calcite veins are highly abundant (the GOI values are approximately 3%~15%), and they mainly developed during or after the filling of calcite veins/quartz veins. The methane and hydrocarbon-bearing brine inclusions are distributed in groups and bands in calcite and quartz minerals.

In sample SXX-15-8, Longmaxi Formation calcite veins, quartz and calcite developed in turn and lack fluorescence. Methane inclusions that are uniformly and densely distributed in calcite and quartz, with a GOI of $\pm 20\%$ (Figure 4A), are extremely abundant. The methane and hydrocarbon-bearing brine inclusions are uniformly densely distributed, grouped and banded in calcite minerals (Figure 4D) or banded in quartz minerals (Figure 4E,F). The hydrocarbon-bearing brine inclusions are polygonal, elliptical and rectangular, with axes ranging from 2 to 15 μm and gas–liquid ratios less than 5% (Figure 5A). Because the methane inclusions are concentrated in “lenses”, the inclusions appear black at the edges and bright white in the middle under single polarized light. Large individual methane inclusions are elliptical and irregular polygons, with axes ranging from 4 to 13 μm , and they are light in the middle and dark around the inclusions under the microscope (Figure 5D). Because the methane inclusions which were formed and filled during the filling of calcite minerals in the calcite microcrack surfaces and quartz minerals have no obvious occurrence relationship with the fracture veins and methane inclusions that are uniformly and densely distributed in calcite, sample SXX-15-8 contains only one stage of oil and gas inclusions.

In sample SX-87 from the Longmaxi Formation calcite veins, quartz and calcite developed in turn, and quartz is replaced by calcite (Figure 4B). Methane inclusions developed after the filling period of calcite minerals, with a GOI of 3%. Specifically, inclusions are distributed in groups and in bands in calcite (Figure 4G) or in bands in quartz (Figure 4H,I). Hydrocarbon-containing brine inclusions show polygonal, elliptical, rectangular and square shapes under a single polarizer with long axes ranging from 2 to 20 μm , and gas–liquid ratios are lower than 5% (Figure 5B). The large individual methane inclusions are elliptical and irregular polygonal and have long axes ranging from 13 to 20 μm (Figure 5E). Because the methane inclusions in the calcite microcrack surfaces and the quartz have no obvious occurrence relationship with the veins, the methane inclusions in the calcite that are distributed in groups were formed and filled after the calcite mineral filling period, so SX-87 contains one stage of oil and gas inclusions.

The calcite veins in the shale in sample DZXX-1-5 of the Longmaxi Formation display no fluorescence, and the methane inclusions developed in the calcite veins, with a GOI of $\pm 3\%$, after the formation of the calcite veins (Figure 4C). The inclusions are mainly distributed in bands of calcite, although some are distributed in groups (Figure 4J–L). Under polarized light, hydrocarbon-containing brine inclusions show polygonal, elliptical and rectangular shapes; the long axes range from 2 to 14 μm , and the gas–liquid ratios are less than 5% (Figure 5C). The methane inclusions are oval, square and irregular polygons, and the individual inclusions are large, with long axes ranging from 2 to 7 μm . Since the methane inclusions in the calcite microfracture surfaces have no obvious relationship with the fracture veins, there is only one stage of oil and gas inclusions in sample DZXX-1-5.

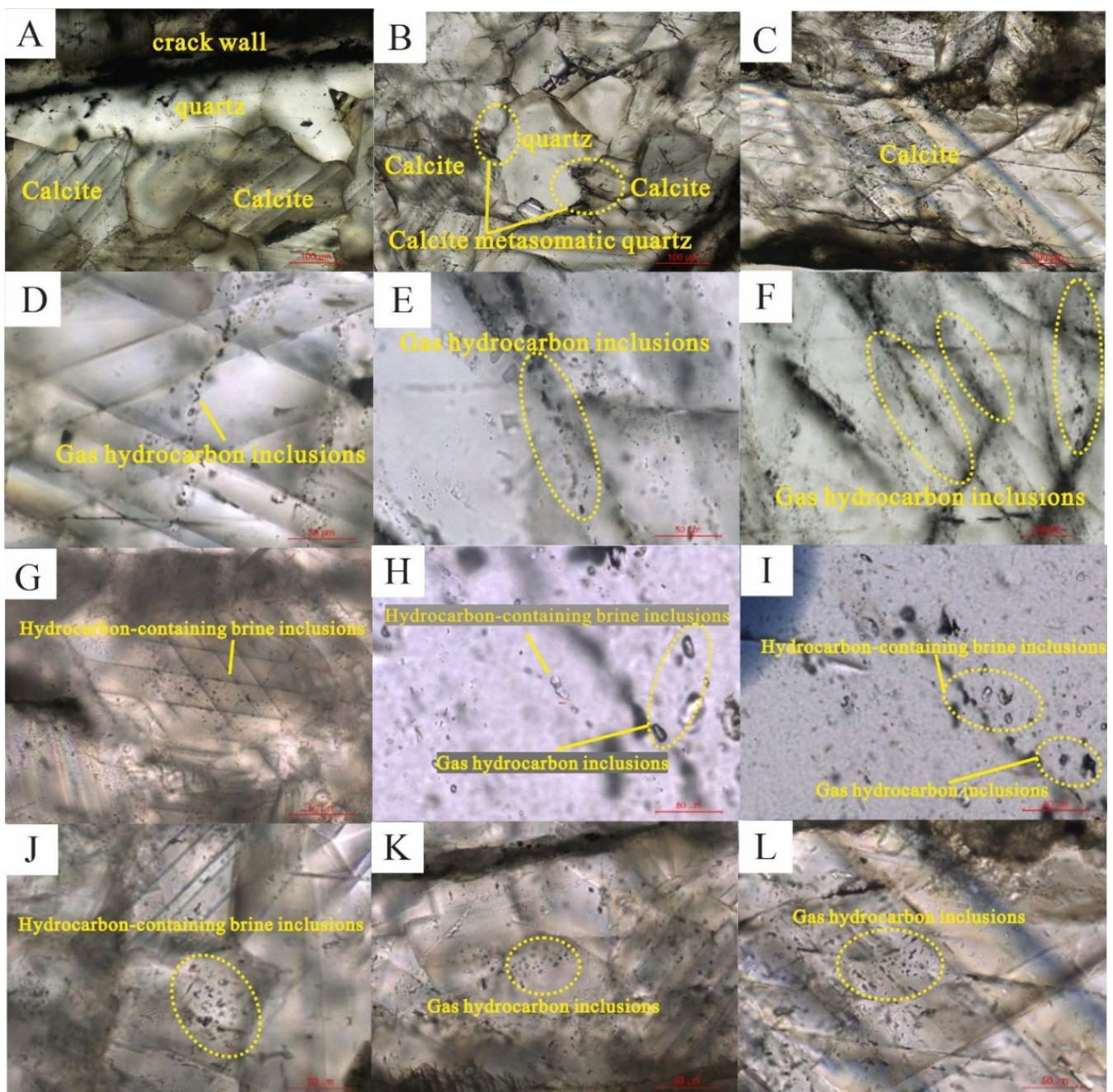


Figure 4. Microscopic characteristics of inclusions and minerals. (A) Carrier of fluid inclusion of SXX-15-8; (B) Carrier of fluid inclusion of SXX-87; (C) Carrier of fluid inclusion of DZXX-1-5; (D) Gas hydrocarbon inclusions of SXX-15-8; (E) Gas hydrocarbon inclusions of SXX-15-8 (F) Gas hydrocarbon inclusions of SXX-15-8; (G) Hydrocarbon-containing brine inclusions of SX-87; (H) Hydrocarbon-containing brine inclusions and Gas hydrocarbon inclusions of SX-87; (I) Hydrocarbon-containing brine inclusions and Gas hydrocarbon inclusions of SX-87; (J) Hydrocarbon-containing brine inclusions of DZXX-1-5; (K) Gas hydrocarbon inclusions of DZXX-1-5; (L) Gas hydrocarbon inclusions of DZXX-1-5.

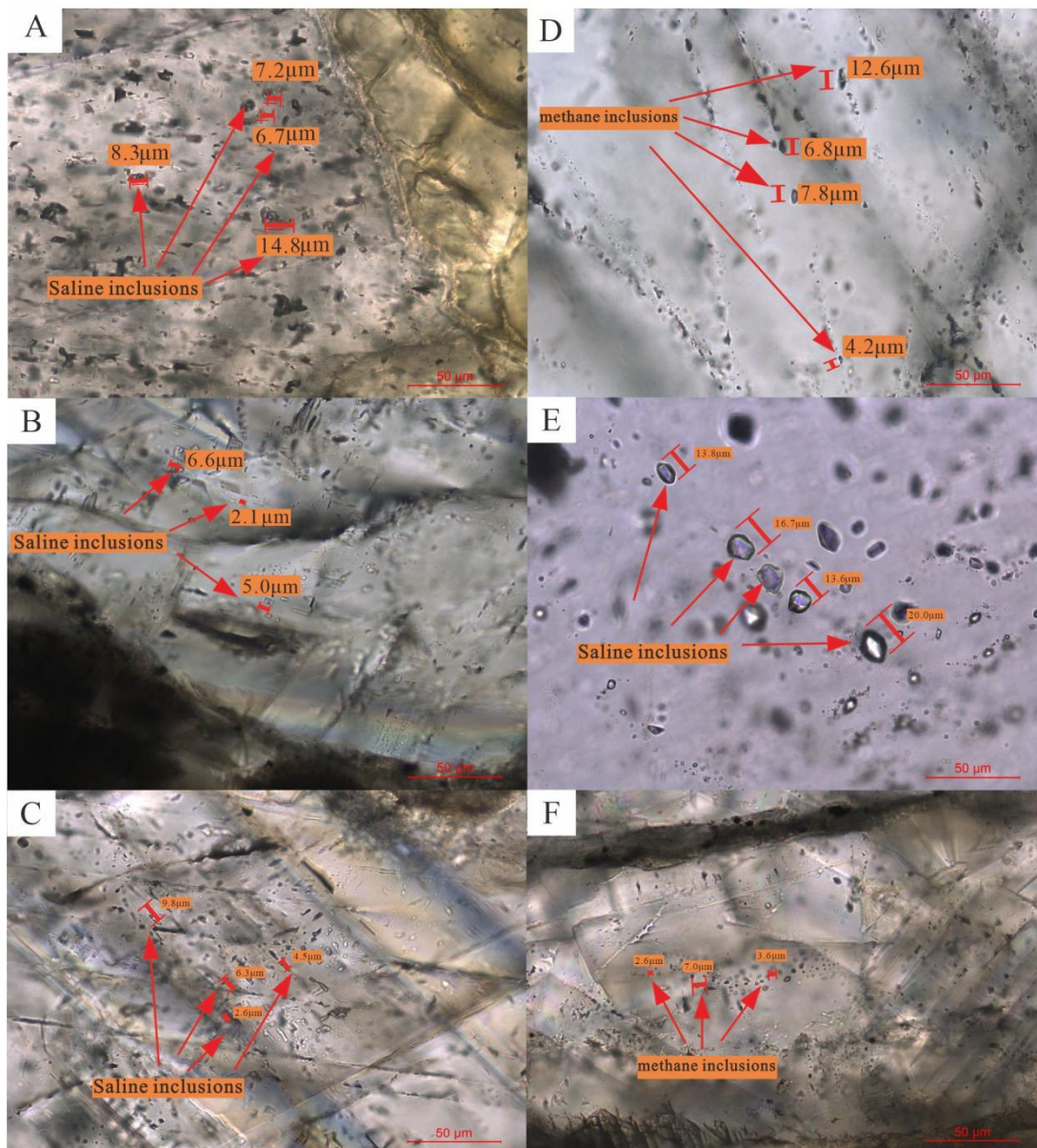


Figure 5. Morphology and production characteristics of brine inclusions and methane inclusions in fracture veins in the western (outcrop) Shixi syncline, the Shixi 1 well and the western Daozhen syncline (outcrop) in northern Guizhou Province. (A) Hydrocarbon-bearing brine inclusions in calcite minerals in sample SXX-15-8 (outcrop), single polarizer; (B) Hydrocarbon-bearing brine inclusions in calcite mineral microfractures in sample SX-87, single polarizer, 1325.04 m; (C) Hydrocarbon-bearing brine inclusions in calcite mineral microfractures in sample DZXX-1-5 (outcrop), single polarizer; (D) Methane inclusions in quartz minerals in sample SXX-15-8 (outcrop), single polarizer; (E) Methane inclusions in quartz microcracks in sample SX-87, single polarizer, 1325.04 m; (F) Methane inclusions in calcite microcracks in sample DZXX-1-5 (outcrop), single polarizer.

4.2. Fluid Inclusion Thermometry and Fluid Filling History

The microthermometry of fluid inclusions includes the homogenization temperature measurements of methane inclusions and gas–liquid two-phase brine inclusions coexisting with methane inclusions. Many single-phase methane inclusions are present around the gas–liquid two-phase brine inclusions in the sample, indicating that the fluid inclusions are trapped in an immiscible two-phase system saturated with methane, and the homogenization temperature of the gas–liquid two-phase brine inclusions can represent the capture

temperature of methane inclusions [52,53]. The homogenization and freezing point temperatures of gas–liquid two-phase brine inclusions in sample SXX-15-8 from the second member of the Longmaxi Formation in the Western Shixi syncline, sample SX-87 from the Longmaxi Formation in the Well SX-1 and inclusions from sample DZXX-1-5 from layer 8 (first member of the Longmaxi Formation) in the western Daozhen syncline were tested. For the selection of test subjects, it was necessary to select long axis lengths of between 2 and 20 μm , for which the gas–liquid ratios were lower than 5%. Inclusions with clear outline and uniformly distributed features were observed, while abnormal inclusions that have been nonuniformly captured were eliminated. Then, the temperature is measured in strict accordance with the test principles of the FIA. The modified conversion formula for the freezing point temperatures and salinities of fluid inclusions in the H_2O -NaCl system revised in [54] was used to calculate the inclusion salinities. It is worth noting that the inclusion salinity is an important parameter reflecting the physicochemical properties of oil and gas reservoir-forming fluids; this parameter can indicate the physicochemical properties and sources of paleofluids and approximately indicate the salinity of paleofluids when inclusions formed [55].

According to the homogenization temperature distribution of fluid inclusions and the relationship between the homogenization temperature and salinity distribution, the oil and gas inclusions of samples SXX-15-8, SX-87 and DZXX-1-5 are all bimodal and are type III inclusions. These results indicate that the inclusions in the above three samples are formed by two phases of fluid filling.

The measured temperature results of inclusions show that there is one stage of oil and gas inclusions that developed in the calcite and quartz veins of sample SXX-15-8 from the Longmaxi Formation and that two periods of continuous fluid filling occurred at the same time. The main homogenization temperature peak of fluid inclusions in the first stage is 150–179 $^{\circ}\text{C}$, with an average of 166 $^{\circ}\text{C}$. The salinity values are 3.23%–21.68%, with an average of 16.95%. These results indicate mainly hydrocarbon-containing brine inclusions and gas hydrocarbon inclusions, which are uniformly dense or banded in calcite minerals. The main homogenization temperature peak of fluid inclusions in the second stage is 190–233 $^{\circ}\text{C}$, with an average of 208 $^{\circ}\text{C}$. The salinity values are 3.23%–21.68%, with an average of 16.76% (Figure 6A,D). Hydrocarbon-containing brine inclusions and gas hydrocarbon inclusions are distributed in bands in calcite and quartz.

There is one stage of oil and gas inclusions that developed in the calcite microcrack surfaces and quartz veins of sample SX-87 from the Longmaxi Formation; this sample shows two periods of continuous fluid filling. The main homogenization temperature peak of fluid inclusions in the first stage is 100–143 $^{\circ}\text{C}$, with an average of 114 $^{\circ}\text{C}$. The salinity values are 4.49%–8.55%, with an average of 5.88%. These results indicate mainly hydrocarbon-containing brine inclusions and gas hydrocarbon inclusions, which are uniformly dense or banded in calcite microcrack surfaces. The main homogenization temperature peak of fluid inclusions in the second stage is 160–230 $^{\circ}\text{C}$, with an average of 183 $^{\circ}\text{C}$. The salinity values are 2.74%–8.68%, with an average of 5.20% (Figure 6B,E). Hydrocarbon-containing brine inclusions are distributed in quartz mineral bands.

In sample DZXX-1-5 from the Longmaxi Formation, there is one stage of oil and gas inclusions in the calcite microcrack surfaces; the sample shows two periods of continuous fluid filling. The main homogenization temperature peak of fluid inclusions in the first stage is 130–170 $^{\circ}\text{C}$, with an average of 148 $^{\circ}\text{C}$. The salinity values are 3.39%–5.56%, with an average of 4.64%. The main homogenization temperature peak of fluid inclusions in the second stage is 192–208 $^{\circ}\text{C}$, with an average of 200 $^{\circ}\text{C}$. The salinity values are 4.34%–4.96%, with an average of 4.52% (Figure 6C,F). Importantly, the above fluid inclusions are all distributed in the calcite microcrack surfaces.

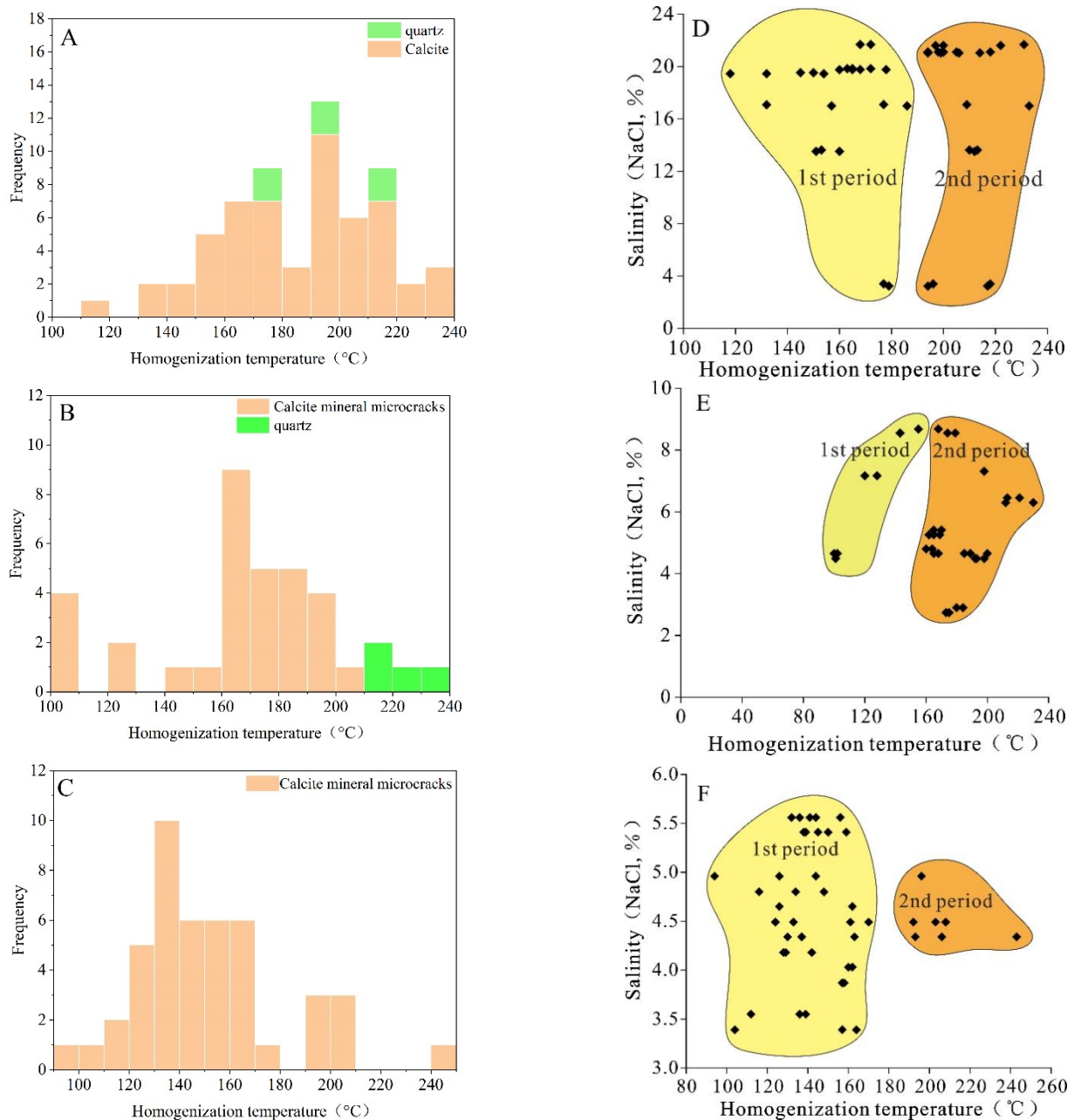


Figure 6. Homogenization temperature and salinity distribution of fluid inclusions from the Wufeng–Longmaxi Formation in northern Guizhou Province. (A) Fluid inclusion homogenization temperature distribution in sample SXX-15-8; (B) fluid inclusion homogenization temperature distribution in sample SX-87; (C) fluid inclusion homogenization temperature distribution in sample DZXX-1-5; (D) fluid inclusion salinity distribution in sample SXX-15-8; (E) fluid inclusion salinity distribution in sample SX-87; (F) fluid inclusion salinity distribution in sample DZXX-1-5.

4.3. Laser Raman Spectral Characteristics of Fluid Inclusions

On the basis of our fluid inclusion study, pure gas-phase methane inclusions with relatively complete and regular morphology were selected for the laser Raman tests. Both the methane inclusions and host minerals in the fracture veins of the Wufeng–Longmaxi Formation have obvious Raman scattering peaks in the laser Raman spectra (Figure 7).

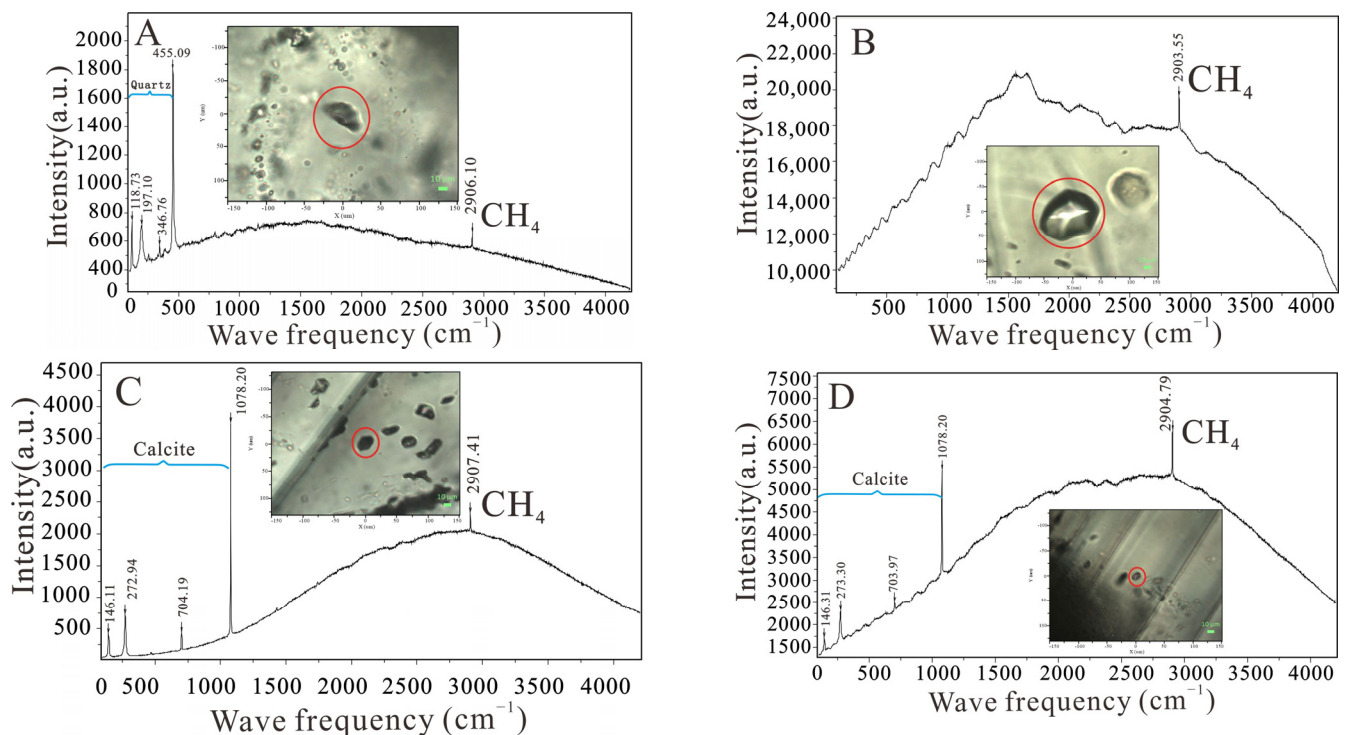


Figure 7. Laser Raman spectra of methane inclusions in the Wufeng–Longmaxi Formation in northern Guizhou Province. (A) Laser Raman spectra of methane inclusions in quartz SXX-15-8, 300 grating; (B) laser Raman spectra of methane inclusions in quartz SX-87, 300 grating; (C) laser Raman spectra of methane inclusions in calcite SBT-WF, 300 grating; (D) laser Raman spectra of methane inclusions in calcite DZXX-1-5, 300 grating.

In these tests, 300 gratings were used to scan the shale samples in the range of 0–4000 cm^{-1} to determine the main mineral types and hydrocarbon inclusion types of the samples. As shown in Figure 6A, the host mineral of sample SXX-15-8 is quartz, which has high laser Raman scattering characteristic peaks and CH_4 characteristic peaks (with a wave frequency of 2906.10 cm^{-1}). Figure 6D shows that the host mineral of DZXX-1-5 is calcite, which has a higher characteristic peak of laser Raman scattering and a characteristic peak of CH_4 (with a wave frequency of 2904.79 cm^{-1}). It is worth noting that the characteristic peaks of methane inclusions in quartz are shifted more than those in calcite.

4.4. Structural Preservation Conditions

Northern Guizhou Province is located in the transitional zone between the trough-like and comb-like deformation zones, where structural conditions are complicated, and different gas contents appear in different structural units. Importantly, the uplift and denudation occurred in the late Yanshanian–Himalayan, which inherited and strengthened the tectonic framework of northern Guizhou Province from the Yanshanian tectonic stage. In other words, the preservation conditions of shale gas reservoirs in the study area were affected or even destroyed by the superposition and reformation of multiple tectonic stages. Therefore, structural preservation conditions are the key to shale gas enrichment and accumulation in northern Guizhou Province.

Due to the multiple tectonic stages and strong strata denudation, the structural units in northern Guizhou Province are mainly “Residual Synclines”, as indicated by the remaining syncline structure after experiencing relatively strong tectonic uplift and denudation, located at the margin of the southeastern Sichuan basin. The data of structural preservation conditions in Table 1 are from the data of drilling, seismic profile and geological maps provided by Guizhou Engineering Research Institute of Oil & Gas Exploration and Development, as well as the field survey data of our research team. The stratigraphic dips,

compaction strength, stresses and other parameters are the key factors affecting physical properties of the reservoir, especially shale gas seepage, which further restricts the establishment of a shale gas accumulation model. As shown in Table 1, the burial depths of the target layer in the Shixi Syncline are 1291.4–1351.7 m, the thickness of the Longmaxi Formation is 28.98 m, the exposed area of the Triassic is 30 km², the angle between the principal stress and fracture strike is 75°, the stratigraphic dips are 0–14° and the distance from the regional fracture is 1.32 km. The burial depths of the target layer in the Daozhen Syncline are 489–597.1 m, the thickness of the Longmaxi Formation is 27.86 m, the angle between the principal stress and fracture strike is 50°, the stratigraphic dips are 4–27° and the distance from the regional fracture is 2.09 km.

Table 1. Structural Preservation Conditions of Different Tectonic Units in Northern Guizhou Province.

Research Area (Syncline)	Structural Style	Burial Depth (m)	Target Layer Thickness Area (m)	Exposed Area of Triassic (km ²)	Acute Angle Between the Principal Stress and Fracture Strike (°)	Stratigraphic Dip (°)	Distance from the Regional Fracture (km)
Shixi	Syncline core reverse fault blocking type	1291.4~1351.7	28.98	30	75	0~14	1.32
Daozhen	reverse fault blocking type	489.0~597.1	27.86	—	50	4~27	2.09
Zhongguan	Normal fault	1080.8~1121.6	21	23.1	—	11~44	1.5
Fuyan	destructive type	1131.2~1141.8	10	49.7	45	49	0.92

5. Discussion

5.1. Fluid Inclusion Paleopressure Recovery

Fluid inclusions record information such as the petrographic characteristics and the ambient fluid temperature and pressure when they are captured, which builds an important “bridge” for reconstructing paleofluid temperature and pressure conditions, paleofluid properties and oil and gas fluid tracing [53,56–61]. To obtain the paleopressure state of the Wufeng–Longmaxi Formation in northern Guizhou Province, the paleopressures of methane inclusions in the fracture veins of samples SXX-15-8, SX-87 and DZXX-1-5 were determined in this paper.

5.1.1. Methane Inclusion Density Calculation

The density of methane inclusions can be determined by the methane inclusion homogenization temperature (*Th*). Our analysis shows that among the 30 methane inclusions tested from sample SXX-15-8, the homogenization temperatures range from −94.8 to −85.1 °C, the homogenization temperatures range from −87.2 to −86.6 °C based on the 30 methane inclusions tested from sample SX-87 and the homogenization temperature is −94.9 °C based on the 6 methane inclusions tested from sample DZXX-1-5. According to Formula (1), the density of methane inclusions can be calculated from the results of the measured homogenization temperatures of methane inclusions [53,62]:

$$\rho(\text{g/cm}^3) = \frac{0.1620506}{(0.288)^r} \quad (1)$$

$$r = \left(1 - \frac{Th + 273.15}{190.6}\right)^{0.2857} \quad (2)$$

where ρ is the density of methane inclusions (g/cm³) and *Th* is the homogenization temperature of methane inclusions (°C). In this study, the homogenization temperature of methane inclusions was substituted into Formulas (1) and (2). The calculation results show that the densities of methane inclusions in the fractured quartz veins in shale samples SXX-15-8 and SX-87 are 0.233–0.286 g/cm³ (the average value is 0.260 g/cm³) and 0.245–0.250 g/cm³ (the average is 0.248 g/cm³), respectively, and the density of methane inclusions in calcite fracture veins in shale sample DZXX-1-5 is 0.286 g/cm³.

5.1.2. Formation Pressure of Methane Inclusions

Hydrocarbon inclusions formed in shale reservoirs, especially natural gas inclusions dominated by methane in oil and gas reservoirs, are important tools for restoring the paleopressure of shale reservoirs due to their wide distribution [56,63–65]. As shown in Section 5.1.1, compared with the critical temperature of the pure methane system ($-82.6\text{ }^{\circ}\text{C}$), the methane inclusions in quartz veins in samples SXX-15-8 and SX-87 and calcite veins in sample DZXX-1-5 have higher densities; thus, they can be called high-density methane inclusions.

On the basis of restoring the density, the trapping pressure of methane inclusions can be calculated by the PVT phase diagram showing the homogenization temperature and density and the pressure and molar volume of supercritical methane inclusions, as comprehensively compiled by Bin Liu et al. [62]. To determine the paleo-trapping pressure of high-density inclusions, it is essential to obtain the trapping temperature of methane inclusions in the sample. In general, the homogenization temperature of hydrocarbon inclusions is lower than the formation temperature, while the homogenization temperature of associated brine inclusions is more accurate than that of hydrocarbon inclusions in the same period that represents the paleo-geo-temperature when the inclusions were formed [66]. Thus, the capture temperature can be directly indicated by the homogenization temperature of brine inclusions coexisting with high-density methane inclusions [67].

According to the PVT phase diagram (Figure 8), the homogenization temperatures of the first-stage hydrocarbon-bearing brine inclusions in sample SXX-15-8 are $150\text{--}179\text{ }^{\circ}\text{C}$, the trapping pressures are $82.35\text{--}92.94\text{ MPa}$, the average burial depth is 4950 m and the formation pressure coefficients are $1.66\text{--}1.88$. In the second fluid filling period, the homogenization temperatures of the hydrocarbon-bearing brine inclusions are $190\text{--}233\text{ }^{\circ}\text{C}$, the trapping pressures are $96.18\text{--}109.71\text{ MPa}$ and the pressure coefficients decrease to $1.63\text{--}1.86$. The homogenization temperatures of the hydrocarbon-bearing brine inclusions in the first period of SX-87 are $100\text{--}143\text{ }^{\circ}\text{C}$, the trapping pressures are $57.35\text{--}70.00\text{ MPa}$ and the pressure coefficients are $1.94\text{--}2.37$. The homogenization temperatures of the second-period hydrocarbon-bearing brine inclusions are $160\text{--}230\text{ }^{\circ}\text{C}$, the corresponding capture pressures are $75.00\text{--}95.59\text{ MPa}$ and the pressure coefficients are $1.29\text{--}1.65$. In sample DZXX-1-5, the homogenization temperatures of the hydrocarbon-bearing brine inclusions in the first period are $130\text{--}170\text{ }^{\circ}\text{C}$, the trapping pressures are $93.82\text{--}108.53\text{ MPa}$ and the pressure coefficients are $2.36\text{--}2.73$. The homogenization temperatures of the second-stage hydrocarbon-bearing brine inclusions are $192\text{--}208\text{ }^{\circ}\text{C}$, the trapping pressures are $119.12\text{--}123.82\text{ MPa}$ and the pressure coefficients are $2.04\text{--}2.12$.

In this study, radioisotope chronology and U-Pb dating of calcite combined with fluid inclusion petrography experiments were used to quantitatively evaluate the burial history and perform a thermal evolution simulation of the burial and uplift denudation processes in order to reveal the controlling effect of tectonic activities on gas reservoirs. Notably, the Shixi syncline is the main object of error analysis. Based on the stable isotopes of fracture veins and in situ U-Pb dating of calcite, it was determined that the late Yanshanian is an important active period of NE and nearly EW trending faults in northern Guizhou Area. The results of a comprehensive analysis of stable isotopes in fractured veins show that: The time limit of NE trending fault activity in northern Guizhou Province is the late Yanshanian ($79.49\text{--}71.34\text{ Ma}$), and the C-O isotopic cross plot shows that oxygen isotopes are mainly distributed in the range of -14.99‰ to -8.97‰ , with an average value of -10.2‰ ; The Z value of paleosalinity for vein formation is 120 ($117.63\text{--}127.12$); and The precipitation temperature of calcite ranges from $137\text{ }^{\circ}\text{C}$ to $174\text{ }^{\circ}\text{C}$, with an average value of $155\text{ }^{\circ}\text{C}$. In conclusion, the NE fracture veins of the Shixi syncline were formed in the late Yanshanian, between $71.34\text{--}79.49\text{ Ma}$.

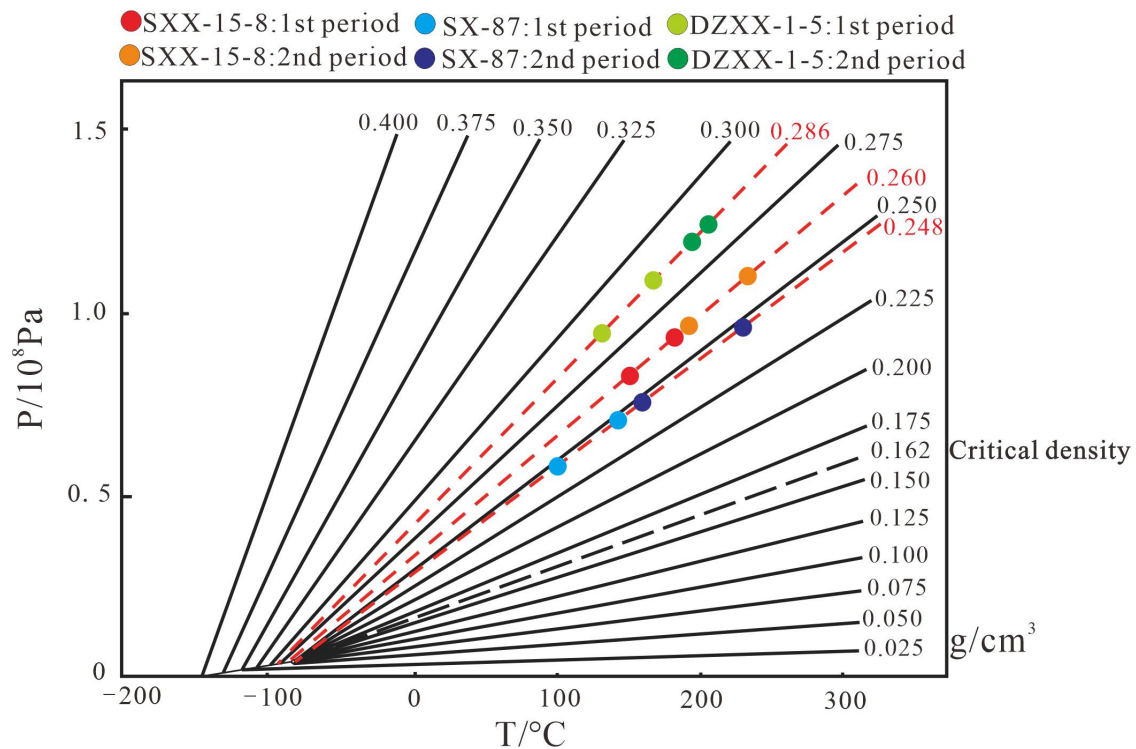


Figure 8. Methane pressure–density–temperature isometric chart (modified from [68]).

On this basis, a new absolute chronological constraint on the duration of fracture activity is provided based on a laser denudation inductively coupled plasma mass spectrometry experiment. The intercept time of the NE trending fault vein in the western Shixi syncline is 82.35 ± 3.6 Ma, and the intercept time of core fracture filling in the Wufeng–Longmaxi Formation in the Shixi 1 well is 84.34 ± 2.2 Ma. The interception time of the above two groups of samples is consistent with the uplift and denudation time, so the opening time of NE trending fault of Shixi 1 well is about the late Yanshanian.

5.2. Pressure Evolution in Shale Gas Reservoirs

The burial–uplift thermal evolution history of the Shixi 1 and the Daoye 1 wells was simulated and reconstructed using Petromod-1D software (Figure 9). In order to build a geological model, it is necessary to obtain geological parameters and important boundary conditions for basin simulation, that is, the formation thickness, denudation thickness, deposition and denudation time of each layer and the relationship between various lithologies and porosity, permeability, seawater depth variations, surface temperature, heat flow value, paleo-geothermal gradient, the thickness of source rock, TOC and hydrocarbon index and so on. On the basis of the above parameters, a geological model was established to simulate the burial history and thermal history. The simulation results show that the Wufeng–Longmaxi Formation in the Shixi 1 and Daoye 1 wells experienced four stages: rapid Caledonian deposition, slow Hercynian uplift, Indosinian–Yanshanian deposition and rapid late Yanshanian–Himalayan uplift.

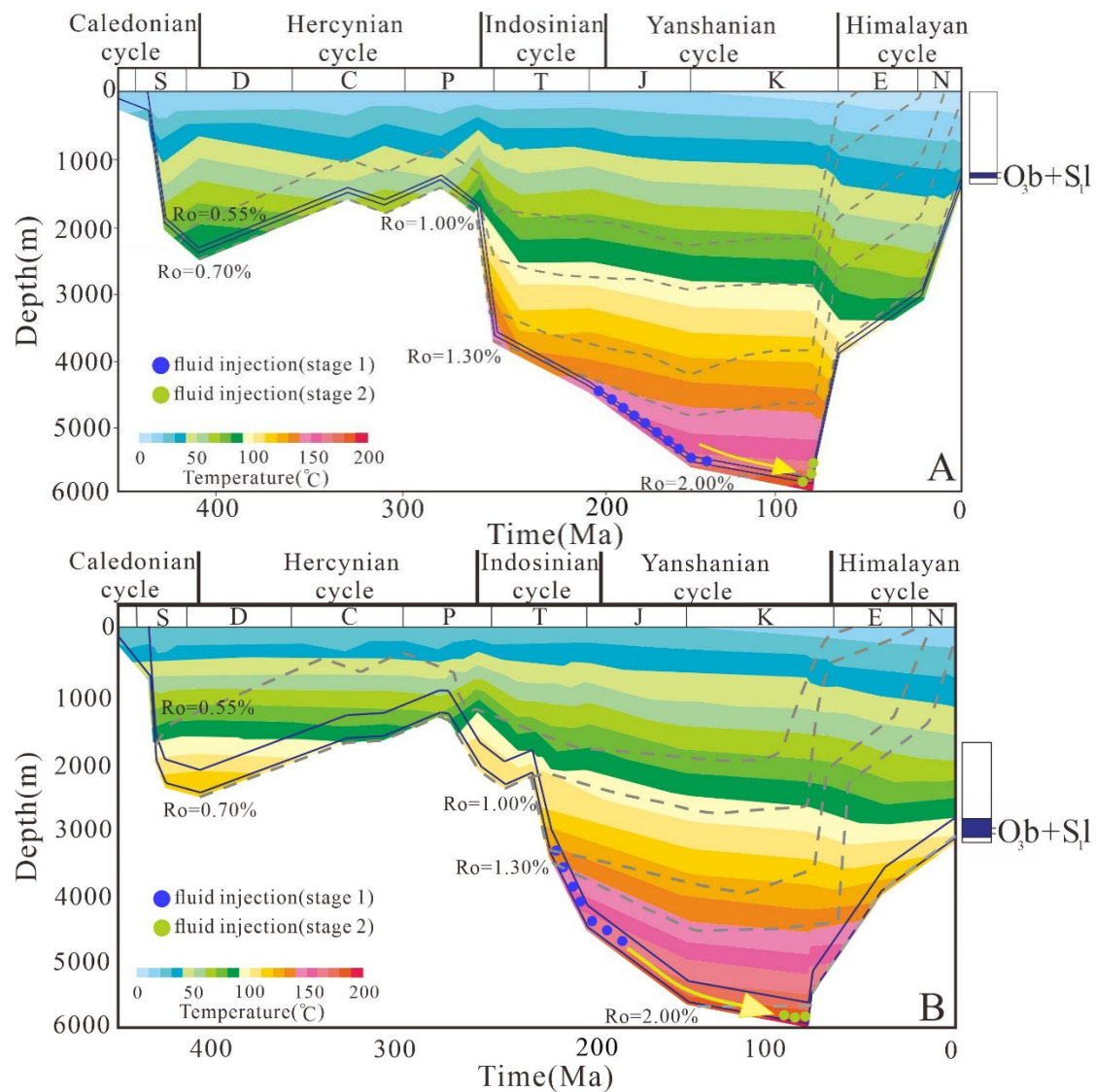


Figure 9. Correlation between the burial history and geothermal history of typical wells in northern Guizhou Province and inclusion capture time. (A) The Shixi 1 well in the Shixi syncline; (B) The Daoze 1 well in the Daozhen syncline.

In terms of the Shixi and Daozhen synclines, the Wufeng–Longmaxi Formation was buried rapidly at the beginning of the Silurian. Subsequently, under the influence of the Caledonian tectonic stage, the burial rate of the whole stratum decreased and began to rise slowly, leading to the denudation of the Carboniferous and Devonian strata in the process. After the Permian, the Wufeng–Longmaxi Formation entered the oil generation window and began to generate a large amount of oil, but the Dongwu tectonic stage in the middle-late Permian resulted in differential uplift and a partial loss of strata. Then, the target layer entered the rapid burial stage. After the Triassic, the strata continued to settle, and the organic matter continued to crack and produce a large amount of gas. Until the late Cretaceous, the settling rate gradually decreased, and the maximum buried depth was close to 6000 m. At the end of Late Cretaceous, multi-stage uplift and denudation occurred and organic gas generation stopped.

According to the data collected in the hydrocarbon generation history of the northern Guizhou Area, the target layer entered the low maturity stage ($R_o = 0.5\%–0.7\%$) in the early Silurian due to the warming effect of rapid deposition. The Permian began to be buried rapidly, and the target layer gradually entered the high maturity stage in the middle-Late

Jurassic, at which time the organic matter generated a lot of oil. In the deep burial period of the Cretaceous, organic matter reached the over-mature stage (the deep high-temperature gas generation stage); its R_o value reached more than 2.0%, causing the organic matter to crack and form gas. After the end of Late Cretaceous, the shale gas reservoir was controlled by uplift and denudation, indicating that the warming process of Wufeng–Longmaxi Formation stopped. Additionally, the corresponding thermal maturity did not increase, with the R_o remaining above 2.0%, although gas generation stopped.

Shale sample SXX-15-8, which has fractured veins, shows two periods of oil and gas charging processes. The capture temperatures of the first period are 150–179 °C. Corresponding to the burial history and thermal evolution history of this area, the capture time of fluid inclusions is closely related to the rapid burial stage of early Yanshan strata in the main gas generation stage. The thermal cracking of liquid hydrocarbons caused an increase in the pore fluid pressure, resulting in formation pressure coefficients as high as 1.66–1.88, indicating a strong overpressure environment. The second-stage capture temperatures are 190–233 °C, which correspond to the stage of rapid uplift and denudation in the late Yanshanian–Himalayan period. In this stage, the organic matter entered the overmature stage, and the hydrocarbon-generating capacity was attenuated. In addition, the overlying pressure during the uplift process decreased, causing the fractures that formed in the early stage to open again, resulting in the formation pressure coefficients decreasing to 1.63–1.86.

Shale sample SX-87, which has fractured veins, shows two periods of oil and gas charging processes. The first period capture temperatures were 100–143 °C, which correspond to the rapid burial during the Indosinian, and the organic matter was in the mature to high-maturity evolution stage. As the formation was rapidly buried, the mechanical compaction was enhanced, resulting in the overburden pressure of the target layer increasing significantly. Therefore, the fracture opening was narrow, and the thermal cracking gas of liquid hydrocarbons continuously increased the pore fluid pressure, raising the formation pressure coefficients to 1.94–2.37, corresponding to a strong overpressure environment. The capture temperatures in the second period were 160–230 °C, which corresponded to the rapid uplift and denudation stage of the late Yanshanian–Himalayan period. The organic matter entered the overmature stage as the hydrocarbon generation capacity decreased, and the overlying pressure decreased during the uplift of the formation, resulting in the reopening of the fractures that formed in the early stage; thus, the formation pressure coefficients decreased to 1.29–1.65.

In addition, two periods of fluid filling processes are shown in the fracture veins in shale sample DZXX-1-5. The first-stage capture temperatures were 130–170 °C, corresponding to the rapid burial of the late Indosinian–early Yanshanian period. The organic matter was in the high-maturity stage, and a large amount of gas was generated after entering the gas window. The thermal cracking gas of liquid hydrocarbons caused the pore fluid pressure to continue to rise, thereby increasing the formation pressure coefficients to 2.36–2.73, indicating a strong overpressure environment. The capture temperatures in the second stage were 192–208 °C, which corresponds to the rapid uplift and denudation stage of the late Yanshanian–Himalayan period. At this time, the organic matter entered the overmature stage, in which the hydrocarbon generation capacity decreased. Moreover, the overlying pressure decreased during the uplift of the formation, and the fractures that formed in the early stage reopened, resulting in the formation pressure coefficients decreasing to 2.04–2.12.

The pressure evolution of the Shixi syncline and the Daozhen syncline was relatively consistent before the uplift in the late Yanshan–Himalayan period, which means both of the target layer of the two tectonic units experienced pressure relief from early Yanshanian to late Yanshanian-early Himalayan and were still in an overpressurized state after the pressure relief. Before or at the beginning of the uplift in the Yanshanian tectonic stage, that is, when the target shale was close to the maximum burial depth, the shale gas layers were in a state of moderate to strong overpressure (Figure 10). Both the Daozhen syncline and the

Shixi syncline shale experienced a rapid uplift stage during the late Yanshanian–Himalayan period, and the starting pressure of the uplift was strongly overpressured. However, there is currently a significant difference in the formation pressure between the two study areas. The data show that the current reservoir pressure coefficient of the Wufeng–Longmaxi Formation in the Daoye 1 well is 0.93, while that of the Wufeng–Longmaxi Formation in the Shixi 1 well is 1.10. This study found that the heterogeneity of the structural preservation conditions under the complex structural transformation that occurred in the late Yanshanian to Himalayan period was the key factor controlling the enrichment of normal-pressure shale gas in the basin margin structural transition zone in northern Guizhou Province.

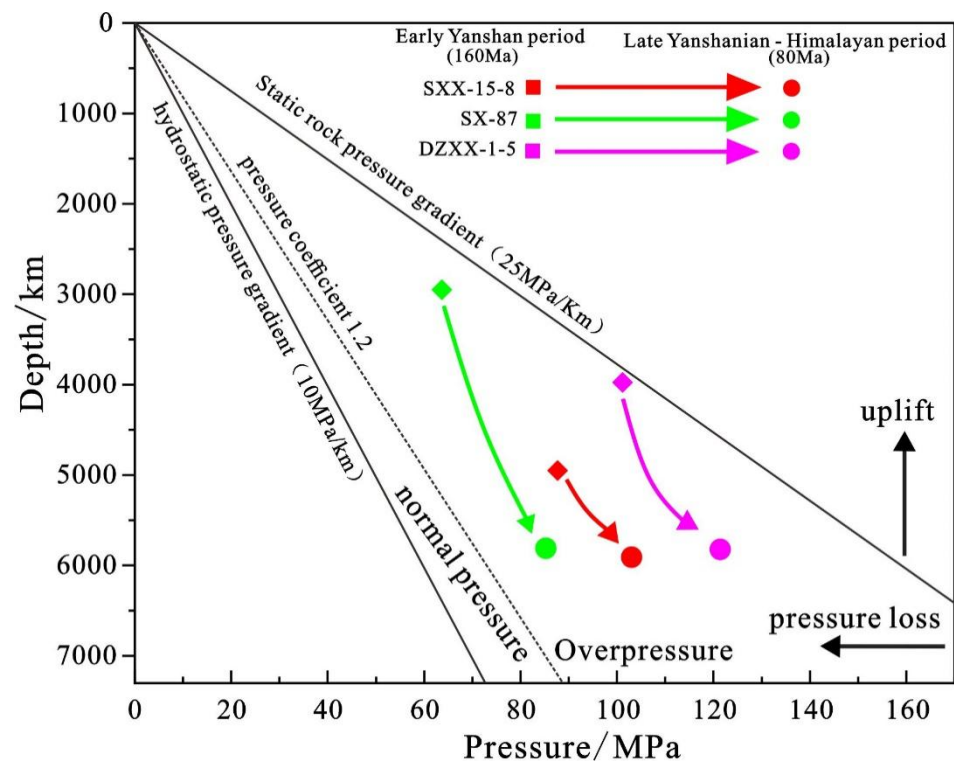


Figure 10. Formation pressure evolution of the Wufeng–Longmaxi Formation in the early Yanshan period and the late Yanshanian–Himalayan period in northern Guizhou Province.

During the accumulation adjustment period from the early Himalayan period to the present, the Wufeng–Longmaxi Formation began to rise substantially under the regional tectonic background, with the reservoir temperature decreasing, which stopped the generation of hydrocarbons at this stage. The pressure evolution mechanism of different tectonic units shown in Figure 10 is as follows: Due to the development of a detachment layer on both sides of the Shixi syncline, a small amount of shale gas escaped along the detachment layer towards the high part of structure. Notably, the dip angle near the Shixi syncline core is relatively gentle (the dip angle is $0\sim 14^\circ$), which is a wide stratum distribution area. Due to the weak structural superposition in the later stage, the buried depth of the target layer is large (1291–1352 m) and the fault sealing is strong (acute angle between the principal stress and fracture strike is 75°), which makes up for the damage of shale gas preservation conditions caused by the large uplift of Shixi syncline during the accumulation and adjustment period, meaning that the overpressure environment was effectively preserved (pressure coefficient is 1.10). As for the Daozhen syncline, under the background of regional tectonics, the strata were greatly deformed, and the region experienced a NW–SSW tectonic extrusion in the early Yanshanian period and a NNE–SSW tectonic extrusion in the late Yanshanian period. The NE-trending structure was restricted by reverse faults, which shifted to an almost SN direction under the action of the tectonic stress field in the late period. Due to

the large degree of structural superposition, the dip angle became larger (the formation dip angle is $4\text{--}27^\circ$), the sealing property of the fault became worse (the acute angle between the principal stress and fracture strike is 50°) and the shallow burial depth (489–597 m) also aggravated the escape of shale gas. At the same time, shale gas could also escape along the detachment layer to the two wings, which eventually led to the Wufeng–Longmaxi Formation leaking to normal pressure (the pressure coefficient is 0.93).

5.3. Mechanism of Shale Gas Reservoir Pressure Evolution

According to previous studies, the overall preservation conditions of shale gas in the Sichuan Basin are strong and have resulted in “preserved sustainable shale gas”, while the preservation conditions of the basin margin structural transition zone are worse than those in the Sichuan Basin, resulting in “dissipated residual shale gas” [45]. In the structural transition belt in northern Guizhou Province, the factors that have led to differences in the preservation conditions of different structural units include the stratum burial depth, fault sealing and its degree of development, stratigraphic dip and structural style (Table 1).

5.3.1. Comprehensive Evaluation of Preservation Conditions

Uplift and denudation caused the shale burial depth to become shallower. In addition, the permeability, diffusion coefficient and desorption rate of shale gas layers increased, and the shale itself became less sealed. Our exploration shows that the greater the burial depth, the better the maintenance of fluid pressure inside the shale. On the other hand, under the action of gas adsorption, the lateral permeability of shale can be reduced and can self-seal, which can slow the lateral migration of shale gas [68]. Specifically, the burial depths of the target layer of the Shixi 1 well are 1291–1352 m, while those of the target layer of Daoye 1 well are only 240–590 m. It is also important that the thickness of the target layer in Shixi 1 (28.98 m) is greater than that in Daoye 1 (27.86 m) (Table 1). Therefore, the fluid pressure of the Wufeng–Longmaxi Formation in Shixi 1 is better maintained, and the degree of self-sealing is higher, which effectively slows the escape of shale gas in the Wufeng–Longmaxi Formation and has enabled the target layer to maintain a high overpressure environment since the late Yanshanian–early Himalayan period.

The degree of fault development affects the quality of the structural preservation conditions. Specifically, in the context of regional tectonic extrusion, the relationship between the maximum principal stress direction of the tectonic stress field and the fault strike affects the sealing of the fault; the greater the acute angle between the two parameters, the better the closure of the fracture [69]. Compared with the Daoye 1 well, Shixi 1 contains more reverse faults, and the angle between the direction of maximum principal stress and the fault strike (75°) is also larger than that of Daoye 1 (50°) (Table 1), which effectively blocked the escape of shale gas in the Wufeng–Longmaxi Formation during the rapid uplift stage since the late Yanshanian–Himalayan period.

The stratigraphic dip also has a certain influence on the escape of shale gas. The dynamic adjustment of shale gas is a necessary process. Under floating action and other factors, shale gas migrates upward, and the upward escape velocity increases as the stratigraphic dip increases [7,70]. The stratigraphic dip of the shale formation in the Shixi syncline is less than 15° , while the stratigraphic dip of the Daozhen syncline is more than 15° . In contrast, the strata that include the Shixi syncline target layer are relatively flat overall (Table 1), which weakens the escape of shale gas. Therefore, a large amount of thermal cracking gas generated during the key accumulation period of shale gas in the Wufeng–Longmaxi Formation in the Shixi syncline is well preserved, as is the overpressure environment, which is further proven by its good gas-bearing properties.

5.3.2. Structural Style

The current tectonic style controls the sealing of deformation structures, such as faults and detachment layers, which, in turn, affects the preservation conditions of the current oil and gas occurrence and the possibility of accumulation. Specifically, to a large extent,

shale gas accumulation requires good sealing. For shale gas accumulations, different structural styles have different shale gas drainage systems and sealing properties [71]. Northern Guizhou Province experienced rapid deposition in the Caledonian period, slow uplift in the Hercynian period, rapid deposition in the Indosinian–late Yanshan period and rapid uplift in the late Yanshan–Himalayan period. Therefore, since the formation of the Yangtze continental core, the province has experienced multiple of tectonic stages and superpositions of caprock deposition, thereby forming the complex and diverse tectonic styles found in the northern Guizhou area today [13]. According to field outcrops, drilling data, seismic profiles and other data, the structural styles of the Shixi syncline and the Daozhen syncline are the “facing thrust structural sealing type” and the “reverse fault lateral blocking type”, respectively (See the cross section shown in Figure 11C). The Shixi 1 well is located in the syncline structure formed by the hedging of two thrust faults, and most of the shale gas in the Wufeng–Longmaxi Formation is accumulated in the footwall of the thrust structure. In the Shixi syncline, the dip angle of the stratum near the synclinal core is relatively flat, which shows a wide and gentle distribution area for strata. The target layer is deeply buried, and the fault sealing is strong, leading to a better blocking effect of shale gas escape (Figure 12a) and a relatively weak degree of structural superposition and transformation in the later stage. In the Daoye 1 well, the target layer in the footwall of the “reverse fault lateral blocking” shale gas reservoir is connected with the tight interlayer in the upper wall, which is laterally blocked by the reverse fault, resulting in shale gas remaining in the footwall of the fault (Figure 12e). However, the shallower the burial depth, the larger the stratigraphic dip; as such, the poor fracture closure led to the escape of a large portion of the Wufeng–Longmaxi Formation shale gas.

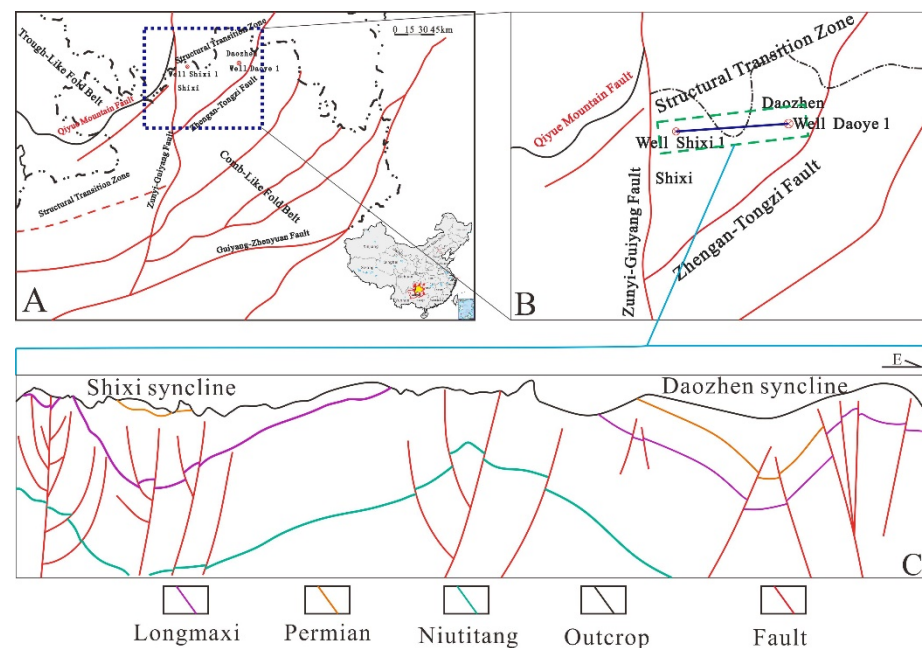


Figure 11. Geological map and profile of the study wells. (A) Geological outline map of the study area; (B) Specific study well location map; (C) Structural profile of the study area.

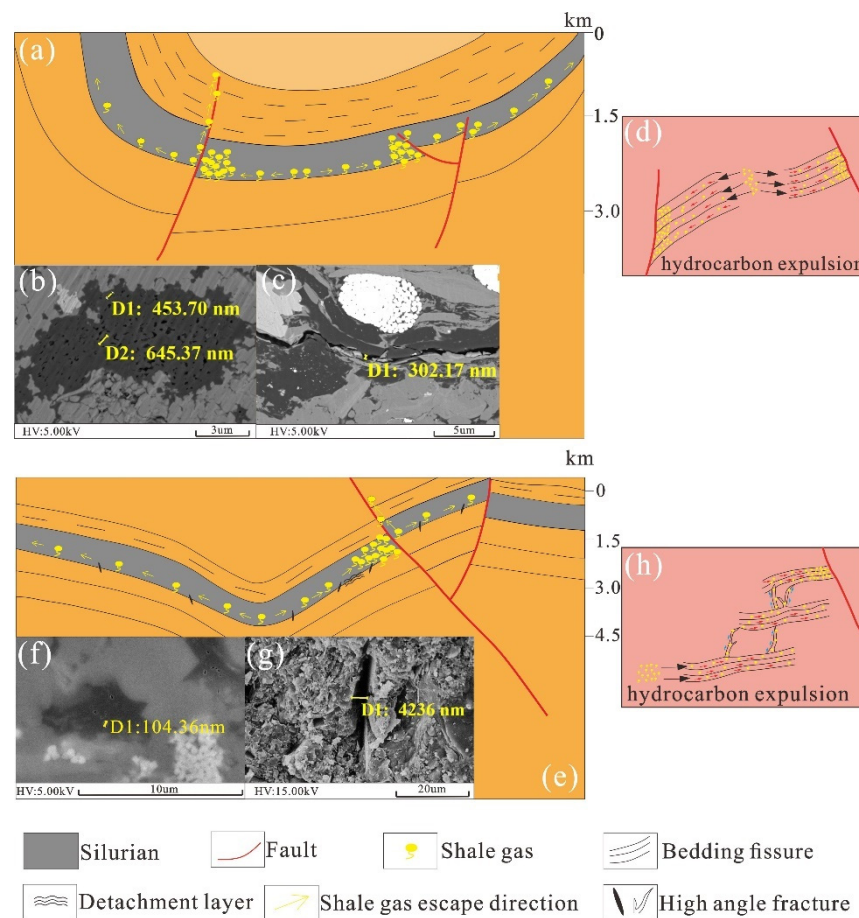


Figure 12. Model of shale gas accumulation in the Shixi and Daozhen synclines in northern Guizhou Province. (a) Shale gas accumulation model in Shixi area; (b) Organic pores of Wufeng—Longmaxi Formation, Well Shixi 1; (c) Micro-fractures of Wufeng—Longmaxi Formation, Well Shixi 1; (d) Microscopic migration patterns of shale gas in Shixi area; (e) Shale gas accumulation model in Daozhen area; (f) Organic pores of Wufeng—Longmaxi Formation, Well Daoye 1; (g) Micro-fractures of Wufeng—Longmaxi Formation, Well Daoye 1; (h) Microscopic migration patterns of shale gas in Daozhen area.

5.4. Shale Gas Differential Enrichment and Accumulation Model of the Basin Margin Structural Transition Zone

During the late Yanshanian–Himalayan period, the study area experienced strong folds and uplifts due to the strong horizontal tectonic compression of plate collision; this period was critical for shale gas preservation. It is worth noting that the basin margin structural transition zone in northern Guizhou Province has undergone multistage tectonic transformations, so the structural evolution and deformation degree of different tectonic units, the time and intensity of strata uplift and denudation and the characteristics of shale gas accumulation and escape are significantly different. As a result, the types of shale gas reservoirs are numerous and diverse, and the enrichment and accumulation patterns of different types of shale gas reservoirs are also significantly different. Based on the pressure evolution, basin burial history, thermal evolution history, structural preservation conditions, typical well anatomy, seismic profiles and shale gas accumulation and escape characteristics, the shale gas enrichment and accumulation models of the Shixi syncline, called the “facing thrust structural sealing type”, and Daozhen syncline, called the “reverse fault lateral blocking type”, were established (Figure 11).

5.4.1. Facing Thrust Structural Sealing Type

Based on the current structural style, the Shixi 1 well is located in the eastern Shixi syncline in the syncline structure formed by the hedging of two thrust faults. Most of the shale gas in the Wufeng–Longmaxi Formation is in the footwall of the hedging structure (Figure 12a).

Based on the generation and dissipation of shale gas in the reservoir under the tectonic background and the characteristics of the spatial structure of the current reservoir, the shale gas accumulation process of the Wufeng–Longmaxi Formation in the Shixi syncline study area can be divided into the following four stages.

The first stage was the shallow burial stage from the Caledonian to early Hercynian, when the Wufeng–Longmaxi Formation was buried to approximately 2500 m after deposition and then slowly uplifted to 1500 m. In this stage, hydrocarbon generation was weak, and faults had not yet developed. The second stage was the initial accumulation stage from the Indosinian period to the early Yanshan period. The target layer was quickly buried below 4000 m, and fractures began to develop as compaction became stronger. The reservoir temperature increased rapidly. In this stage, the shale organic matter entered the gas window and began to generate thermally degraded gas. Note that the strong compaction increased the vertical load of the reservoir, resulting in abnormally high pressures (1.94–2.37). The third stage was the main accumulation period from the late Yanshanian to the early Himalayan period. In the late Yanshanian, the target layer was buried to its greatest depth and reached the highly overmature stage. A large number of liquid hydrocarbons were cracked into dry gas as a large number of organic pores formed (Figure 12b). Note that the increase in the reservoir temperature and the rapid expansion of fluid volume maintained the effective maintenance of the overpressure environment (the pressure coefficients were 1.29–1.65), and a large number of microfractures are also visible in the reservoir (Figure 12c). In the early Himalayan stage, the target layer began to be uplifted, and the fault formed a typical hedging structure under strong tectonic action. The formation pressure of the target formation in the footwall of the reverse fault was higher, leading to underdeveloped induced fractures, and large-scale shale gas escape did not easily occur. As a result, a large amount of shale gas accumulated in the footwall of the hedging structure. The fourth stage was the accumulation adjustment period from the early Himalayan to the present. The Wufeng–Longmaxi Formation began to uplift significantly under the regional tectonic background, the reservoir temperature decreased and hydrocarbon generation stopped. Due to the development of detachment layers on both sides of the syncline, some shale gas escaped along the detachment layers to the higher position of the structure. The stratum dip angle near the syncline core is relatively gentle (the dip angles of the strata are 0–14°). The faults are mainly NE and NNE. The target layer is deeply buried (1291–1352 m). Because the faults have strong sealing properties (the acute angle between the principal stress and the fault strike is 75°), the overpressure environment is effectively preserved (the pressure coefficient is 1.10). Under better sealing conditions for shale gas escape, organic pores and microfractures are also effectively preserved (Figure 12b,c). As shown in Figure 12d, the Shixi syncline experienced large-scale uplift and erosion during the late Yanshanian–Himalayan period, and the target layer was uplifted to 1500–2000 m, causing most of the bedding seams to open. It is worth noting that the shale gas moved along the bedding seams to the dominant structural position until it was blocked by the large thrust fault, where the shale gas was relatively enriched. In summary, the shale gas of the Wufeng–Longmaxi Formation in the Shixi 1 well was weakly adjusted and reformed in the later period, which is conducive to the enrichment and accumulation of shale gas.

5.4.2. Reverse Fault Lateral Blocking Type

Based on the current structural style, the target layer in the footwall of the Daozhen syncline “reverse fault lateral blocking type” shale gas reservoir is connected with the tight interlayer in the upper wall. Due to lateral blocking by reverse faults, shale gas is retained

in the footwall of the fault (Figure 12e). Overall, shale gas is blocked by faults, and the weakening of the lateral migration of shale gas causes it to accumulate.

The shale gas accumulation process of the Wufeng–Longmaxi Formation in the Daozhen syncline study area can also be divided into four stages in the context of multi-phase complex tectonic stage.

Similar to the Shixi syncline, the Daozhen syncline also experienced four stages: the shallow burial period, an initial accumulation period, a main accumulation period and an accumulation adjustment period. The Wufeng–Longmaxi Formation shale entered a high-maturity evolution stage from the Indosinian to the early Yanshanian initial accumulation period, which generated a large amount of thermally degraded gas. The strong compaction of the overlying stratum and the thermal pressurization of the fluid increased the pressure coefficients of the target layer to 2.36–2.73, forming a strong overpressure environment. Large-scale reverse faults developed in this stage, and shale gas began to accumulate in the footwall of the fault. Upon entering the main accumulation stage from the late Yanshanian to the early Himalayan period, the stratum burial depth reached its maximum value, shale organic matter reached the high-overmature stage and a large amount of thermal cracking gas was generated. A large amount of shale gas accumulated in the footwall of the reverse fault, and a large number of organic pores also formed, while the microfractures remained underdeveloped. The increase in the reservoir temperature and the rapid expansion of fluid volume led to the effective maintenance of the overpressure environment (the pressure coefficients were 2.04–2.12). From the early Himalayan period to the present, the strata began to be uplifted and denuded rapidly, and the thermal evolution of organic matter tended to stop with the weakening of the hydrocarbon generation capacity. The strata were greatly deformed, and the region experienced NW–SE-trending compression in the early Yanshan period and NNE–SSW-trending structural compression in the late Yanshan period. The NE-trending structure was restricted by the reverse fault, which deflected from NE-trending to nearly SN-trending under the action of the late tectonic stress field, and a small number of NW-trending faults developed locally. Due to the large degree of structural superposition and transformation, the dip angle of the formation became larger (the dip angles of the formation are 4–27°), the sealing of the fault became worse (the acute angle between the principal stress and the fault strike is 50°) and the shallower burial depth (the burial depths of the formation are 240–590 m) intensified the escape of shale gas. Eventually, the pressure in the Wufeng–Longmaxi Formation was released to normal pressure (the pressure coefficient was 0.93), and the poor preservation conditions also damaged the organic pores and microcracks in the target layer (Figure 12f). In addition, the microfractures in the reservoir accelerated the release of shale gas to a certain extent (Figure 12g). As shown in Figure 12h, the target layer was uplifted to 3000–3300 m during the late Yanshanian–Himalayan, leading to a decrease in the sealing of the bedding seams to a certain extent. Additionally, the development of more high-angle fractures also promoted the vertical migration of shale gas. Along the bedding seams and high-angle fractures, the shale gas moved outward via vertical–horizontal union until it was blocked by the large reverse fault and accumulated in large quantities. In summary, the shale gas in the Wufeng–Longmaxi Formation in the Daoye 1 well was subject to strong adjustment and transformation in the later stage, which was more detrimental to shale gas enrichment and accumulation than what occurred in the Shixi 1 well.

5.5. Guiding Significance of Exploration and Development

The exploration and development of shale gas in North America shows that shale lithofacies analysis is a key and fundamental step to evaluate shale gas reserves, shale fracturing and shale gas productivity. Notably, the effectiveness of hydraulic fracturing is mainly affected by the mechanical properties of rocks, which is closely related to mineral composition, present stress and the horizontal stress difference coefficient. Under the combined action of a larger acute angle between the principal stress and the fracture strike of the Shixi syncline (75°), more brittle mineral content, a better overpressure environment

(Pressure coefficient is 1.10), an extensive and complex fracture network was more easily generated and remained open in the development process.

6. Conclusions

1. One-stage oil and gas inclusions are present in the Wufeng–Longmaxi Formation shale veins in both the Shixi syncline and Daozhen syncline. According to the homogenization temperature distribution of fluid inclusions and the relationship between the homogenization temperature and salinity distribution, the homogenization temperature distributions of samples SXX-15-8, SX-87 and DZXX-1-5 are bimodal, indicating class III inclusions, which all formed by two-phase fluid filling.
2. The Wufeng–Longmaxi Formations in the Shixi and Daozhen synclines both experienced strong overpressure during the first stage of the critical accumulation period (210–150 Ma) and a pressure release during the second stage of the critical accumulation period (95–80 Ma). The difference is that the Wufeng–Longmaxi Formation in the Shixi syncline continued to release pressure, resulting in weak overpressure, since the Himalayan period, while the Wufeng–Longmaxi Formation in Daozhen syncline continued to release pressure, reaching a normal pressure since the Himalayan period. With the destruction of the pressure system of the Daozhen syncline, the preservation conditions and pore structure were destroyed to a great extent.
3. Compared with the degree of thermal evolution and the characteristics of reservoir space development, the heterogeneity of the preservation conditions of different tectonic units caused by structural superimposition since the late Yanshanian–Himalayan period are the key factors controlling the accumulation and enrichment of normal-pressure shale gas in northern Guizhou Province. The Wufeng–Longmaxi Formation in the Shixi syncline has a deeper burial depth (1291.4–1351.7 m), a smaller dip angle (0–14°), a stronger fault sealing ability (the acute angle between the principal stress and fracture strike is 75°) and a higher development degree of organic pores and microfractures. The tectonic style is the “facing thrust structural sealing type”, with strong fault sealing, which is more conducive to the effective preservation of shale gas.
4. Both the Shixi syncline and Daozhen syncline experienced four shale gas accumulation stages: the shallow burial period (Caledonian), an initial accumulation period (Hercynian), a main accumulation period (Indosinian–early Yanshanian) and an accumulation adjustment period (Himalayan to the present). The large-scale uplift of the region and the difference in tectonic stress during this period led to a great change in the characteristics of fault development, the stratigraphic dip, the burial depth of the target layer and the sealing of the faults, which prompted the differential accumulation and escape of shale gas. The Shixi syncline and Daozhen syncline are described by the “facing thrust structural sealing type” and “reverse fault lateral blocking type” shale gas enrichment and accumulation models, respectively.

Author Contributions: Conceptualization, X.L.; methodology, W.D., X.F., Z.J. and Q.L.; software, X.L.; validation, Z.J. and Q.L.; formal analysis, X.L.; investigation, X.L., W.D., X.F., F.S., Y.C., Y.W., Z.J. and Q.L.; resources, W.D.; data curation, X.L.; writing—original draft preparation, X.L.; writing—review and editing, Z.J. and Q.L.; visualization, X.L.; supervision, Z.J. and Q.L.; project administration, X.L.; funding acquisition, W.D. and X.F. All authors have read and agreed to the published version of the manuscript.

Funding: This research was funded by [The National Natural Science Foundation of China] grant number [41602233], [The Science Foundation for top-notch innovative talents of China University of Petroleum, Beijing] grant number [2462017BJB07] and [The Guizhou Geological Exploration Foundation] grant number [208-9912-JBN-L1D7].

Data Availability Statement: Not applicable.

Acknowledgments: This work was supported by the National Natural Science Foundation of China (No. 41602233), the Science Foundation for top-notch innovative talents of China University of Petroleum, Beijing (No. 2462017BJB07), and the Guizhou Geological Exploration Foundation (No. 208-9912-JBN-L1D7).

Conflicts of Interest: The authors declare no competing financial interest.

References

1. Wang, S.Z. The Tectonic Characteristics of Changning Area, South of Sichuan and Crack Characteristics of Longmaxi Formation of Silurian System. Master's Thesis, Chengdu University of Technology, Chengdu, China, 2014.
2. Yang, R.; He, S.; Yi, J.; Hu, Q. Nano-scale pore structure and fractal dimension of organic-rich Wufeng-Longmaxi shale from Jiaoshiba area, Sichuan Basin: Investigations using FE-SEM, gas adsorption and helium pycnometry. *Mar. Pet. Geol.* **2016**, *70*, 27–45. [[CrossRef](#)]
3. Guo, X.S.; Hu, D.F.; Wei, Z.H.; Li, Y.P.; Wei, X.F. Discovery and exploration of Fuling shale gas field. *China Pet. Explor.* **2016**, *21*, 24.
4. Ma, X.H.; Xie, J. The progress and prospects of shale gas exploration and exploitation in southern Sichuan Basin, NW China. *Pet. Explor. Dev.* **2018**, *45*, 161–169. [[CrossRef](#)]
5. Xing, L.; Gaocheng, W.; Jiehui, Z.; Honglin, S.; Chen, L.; Zhaofeng, L.; Zhengyu, X.; Zhao, Z.; Deqi, L.; Yajun, J.; et al. High-efficiency integrated shale gas development model of Zhaotong National Demonstration Zone and its practical enlightenment. *China Pet. Explor.* **2017**, *22*, 29.
6. Liu, N.Z.; Wang, G.Y. Shale gas sweet spot identification and precise geo-steering drilling in Weiyuan Block of Sichuan Basin, SW China. *Pet. Explor. Dev.* **2016**, *43*, 1067–1075. [[CrossRef](#)]
7. Jiang, Z.; Song, Y.; Tang, X.L.; Li, Z.; Wang, X.M.; Wang, G.Z.; Xue, Z.X.; Li, X.; Zhang, K.; Chang, J.Q.; et al. Controlling factors of marine shale gas differential enrichment in southern China. *Pet. Explor. Dev.* **2020**, *47*, 661–673. [[CrossRef](#)]
8. Yang, W.; Cai, J.F.; Wang, Q.Y.; Cui, Z.; Cui, Z.; Xu, L.; Li, L.; Gu, X.; Wang, J. The controlling effect of organic matter coupling with organic matter porosity on shale gas enrichment of the Wufeng-Longmaxi marine shale. *Pet. Sci. Bull.* **2020**, *5*, 148–160.
9. Pollastro, R.M. Total petroleum system assessment of undiscovered resources in the giant Barnett Shale continuous (unconventional) gas accumulation, Fort Worth Basin, Texas. *AAPG Bull.* **2007**, *91*, 551–578. [[CrossRef](#)]
10. Guo, X.S. Rules of two-factor enrichment for marine shale gas in southern China: Understanding from the Longmaxi Formation shale gas in Sichuan Basin and its surrounding area. *Acta Geol. Sin.* **2014**, *88*, 1209–1218.
11. Guo, X.S.; Hu, D.F.; Li, Y.P.; Liu, R.B.; Wang, Q.B. Geological features and reservoiring mode of shale gas reservoirs in Longmaxi Formation of the Jiaoshiba area. *Acta Geol. Sin. Engl. Ed.* **2014**, *88*, 1811–1821. [[CrossRef](#)]
12. Zhi, Y.; Caineng, Z.; Songtao, W.; Senhu, L.; Songqi, P.; Xiaobing, N.; Guangtian, M.; Zhenxing, T.; Guohui, L.; Jiahong, Z.; et al. Formation, distribution and resource potential of the “sweet areas (sections)” of continental shale oil in China. *Mar. Pet. Geol.* **2019**, *102*, 48–60. [[CrossRef](#)]
13. Yan, J.F. The Shale Gas Accumulation Conditions and Distribution Characteristics of Black Shales in the Upper Ordovician Wufeng Formation—Lower Silurian Longmaxi Formation of northern Guizhou. Ph.D. Thesis, Chengdu University of Technology, Chengdu, China, 2017.
14. Sun, W.; Zuo, Y.; Wang, S.; Wu, Z.; Liu, H.; Zheng, L.; Lou, Y. Pore structures of shale cores in different tectonic locations in the complex tectonic region: A case study of the Niutitang Formation in Northern Guizhou, Southwest China. *J. Nat. Gas Sci. Eng.* **2020**, *80*, 103398. [[CrossRef](#)]
15. Ma, Y.S.; Cai, X.Y.; Zhao, P.R. China's shale gas exploration and development: Understanding and practice. *Pet. Explor. Dev.* **2018**, *45*, 561–574. [[CrossRef](#)]
16. Zhao, W.; Li, J.; Yang, T.; Wang, S.; Huang, J. Geological difference and its significance of marine shale gases in South China. *Pet. Explor. Dev.* **2016**, *43*, 499–510. [[CrossRef](#)]
17. Wu, J.; Chen, X.Z.; Liu, W.P.; Wu, W.; Gao, Y.; Luo, C.; Deng, B.; Zhou, Z. Fluid Activity and Pressure Evolution Process of Wufeng-Longmaxi Shales, Southern Sichuan Basin. *Earth Sci.* **2022**, *47*, 518–531.
18. Guo, T.L. Evaluation of Highly Thermally Mature Shale-Gas Reservoirs in Complex Structural Parts of the Sichuan Basin. *J. Earth Sci.* **2013**, *24*, 863–873. [[CrossRef](#)]
19. Chen, Z.Y.; Song, Y.; Jiang, Z.X.; Liu, S.B.; Li, Z.; Shi, D.S.; Yang, W.; Yang, Y.D.; Song, J.A.; Gao, F.L.; et al. Identification of organic matter components and organic pore characteristics of marine shale: A case study of Wufeng-Longmaxi shale in southern Sichuan Basin, China. *Mar. Pet. Geol.* **2019**, *109*, 56–69. [[CrossRef](#)]
20. Li, X.; Jiang, Z.X.; Wang, P.F.; Song, Y.; Li, Z.; Tang, X.L.; Li, T.W.; Zhai, G.Y.; Bao, S.J.; Xu, C.L.; et al. Porosity-preserving mechanisms of marine shale in Lower Cambrian of Sichuan Basin, South China. *J. Nat. Gas Sci. Eng.* **2018**, *55*, 191–205. [[CrossRef](#)]
21. Zhang, K.; Jiang, Z.; Xie, X.; Gao, Z.; Liu, T.; Yin, L.; Jia, C.; Song, Y.; Shan, C.A.; Wu, Y. Lateral percolation and its effect on shale gas accumulation on the basis of complex tectonic background. *Geofluids* **2018**, *2018*. [[CrossRef](#)]
22. Aplin, A.; Macleod, G.; Larter, S.; Pedersen, K.; Sorensen, H.; Booth, T. Combined use of Confocal Laser Scanning Microscopy and PVT simulation for estimating the composition and physical properties of petroleum in fluid inclusions. *Mar. Pet. Geol.* **1999**, *16*, 97–110. [[CrossRef](#)]

23. Hansen, S.B.; Berg, R.W.; Stenby, E.H. How to determine the pressure of a methane-containing gas mixture by means of two weak Raman bands, $\nu(3)$ and $2\nu(2)$. *J. Raman Spectrosc.* **2002**, *33*, 160–164. [[CrossRef](#)]
24. Bourdet, J.; Pironon, J.; Levresse, G.; Tritlla, J. Petroleum type determination through homogenization temperature and vapour volume fraction measurements in fluid inclusions. *Geofluids* **2008**, *8*, 46–59. [[CrossRef](#)]
25. Ping, H.; Thiery, R.; Chen, H. Thermodynamic modeling of petroleum inclusions: The prediction of the saturation pressure of crude oils. *Geofluids* **2011**, *11*, 328–340. [[CrossRef](#)]
26. Chen, Y.; Steele MacInnis, M.; Ge, Y.J. Synthetic saline-aqueous and hydrocarbon fluid inclusions trapped in calcite at temperatures and pressures relevant to hydrocarbon basins: A reconnaissance study. *Mar. Pet. Geol.* **2016**, *76*, 88–97. [[CrossRef](#)]
27. Xu, Z.; Liu, L.; Wang, T.; Wu, K.; Gao, X.; Dou, W.; Xiao, F.; Zhang, N.; Song, X.; Ji, H. Application of fluid inclusions to the charging process of the lacustrine tight oil reservoir in the Triassic Yanchang Formation in the Ordos Basin, China. *J. Pet. Sci. Eng.* **2017**, *149*, 40–55. [[CrossRef](#)]
28. Guo, T.L.; Zhang, H.R. Formation and enrichment mode of Jiaoshiha shale gas field, Sichuan Basin. *Pet. Explor. Dev.* **2014**, *41*, 28–36. [[CrossRef](#)]
29. Chang, D.S.; Han, B.; Zhu, D.X.; Jiang, L.W.; Wang, Y.L.; Zhou, C.J.; Cao, L.L.; Li, Y. Control of Yanshanian movement on shale gas preservation conditions: A case study on the Longmaxi Formation shale gas in Taiyang-Haiba Block of northern Yunnan and Guizhou. *Nat. Gas Ind.* **2021**, *41*, 45–50.
30. Pan, L.; Xu, Z.X.; Li, R.B.; Zou, Y.T. Basement Fault Characterization and Hydrocarbon Accumulation in Fuling of Southeastern Sichuan. *Spec. Oil Gas Reserv.* **2020**, *27*, 19–25.
31. Ran, T.; Tan, X.F.; Chen, H.; Wang, J.; Jiang, W.W.; Chen, Q.; Zeng, C.L.; Chen, C. Geological features of shale gas accumulation in the Lower Silurian Longmaxi Formation, Southeast Chongqing. *Pet. Geol. Recovery Effic.* **2017**, *24*, 17–26. [[CrossRef](#)]
32. Wang, S.L. The Influence of Structure on Accumulation of Shale Gas in Lower Cambrian Niutitang Formation in Cen’gong, Guizhou. Master’s Thesis, Guizhou University, Guiyang, China, 2017.
33. Yang, W.; Xu, L.; Chen, D.; Jiang, Z.; Zhang, Z.; Hao, B.; Zuo, R.; Wang, Q.; Chen, R. How argillaceous reservoirs exhibit better quality than silty mudstones? Anomalous behavior of shale gas-bearing properties of continental fine-grained sediments in Southwest China and its possible forcing mechanisms. *Pet. Sci.* **2021**, *18*, 1589–1610. [[CrossRef](#)]
34. Ji-Gao, L.E.N.G.; Da-Jian, G.O.N.G.; Fei, L.; Feng, L.I. Analyses on the shale gas exploration prospect of the Niutitang Formation in northeastern Guizhou Area. *Earth Sci. Front.* **2016**, *23*, 29.
35. Yang, R.; Chen, W.; Zhou, R. Characteristics of organic-rich shale and exploration area of shale gas in Guizhou Province. *Nat. Gas Geosci.* **2012**, *23*, 340–347.
36. Hai-quan, Z.H.A.N.G.; Qian, Y.; Yu-xi, L.I.; Jian-fei, Y.A.N.; Wei, L.I.U.; Yu-peng, M.E.N.; Ping, Y.A.N.G. Explorative prospect of shale gas of lower Silurian in middle-upper Yangtze area. *Xinjiang Pet. Geol.* **2011**, *32*, 353.
37. Li, X.; Li, Y.; Li, J.; Zou, X.; Guo, M.; Wang, Z.; Zhang, X.; Wang, F. Characteristics of pore structures from the Lower Paleozoic shale gas reservoirs in northern Guizhou, South China. *J. Nat. Gas Geosci.* **2020**, *5*, 241–253. [[CrossRef](#)]
38. Gao, Z.; Li, B.B.; Li, J.H.; Jia, L.D.; Wang, Z.H. Adsorption characteristics and thermodynamic analysis of shale in northern Guizhou, China: Measurement, modeling and prediction. *Energy* **2023**, *262*, 125433. [[CrossRef](#)]
39. Wu, Z.; Tang, M.; Zuo, Y.; Lou, Y.; Wang, W.; Liu, H.; Sun, W. Acoustic emission-based numerical simulation of tectonic stress field for tectoclase prediction in shale reservoirs of the northern Guizhou area, China. *Energy Geosci.* **2022**, *3*, 436–443. [[CrossRef](#)]
40. Jiang, X.F.; Deng, S.C.; Li, H.B.; Zuo, H. Characterization of 3D pore nanostructure and stress-dependent permeability of organic-rich shales in northern Guizhou Depression, China. *J. Rock Mech. Geotech. Eng.* **2022**, *14*, 407–422. [[CrossRef](#)]
41. Zhou, M.; Liang, Q. Petroleum geological conditions of lower assemblage in Qianzhong uplift and peripheral regions. *Mar. Orig. Pet. Geol.* **2006**, *11*, 17–24.
42. Zhou, S.; Yan, G.; Xue, H.; Guo, W.; Li, X. 2D and 3D nanopore characterization of gas shale in Longmaxi formation based on FIB-SEM. *Mar. Pet. Geol.* **2016**, *73*, 174–180. [[CrossRef](#)]
43. He, Q.; Dong, T.; He, S.; Zhai, G.Y. Methane adsorption capacity of marine-continental transitional facies shales: The case study of the Upper Permian Longtan Formation, northern Guizhou Province, Southwest China. *J. Pet. Sci. Eng.* **2019**, *183*, 106406. [[CrossRef](#)]
44. Chang, T.L. Study on the Accumulation Conditions of Shale Gas in Longmaxi Formation in Northern Guizhou. Master’s Thesis, Guizhou University, Guiyang, China, 2016.
45. Hu, D.F. Main controlling factors on normal pressure shale gas enrichments in Wufeng-Longmaxi Formations in synclines, southeastern Sichuan Basin. *Nat. Gas Geosci.* **2019**, *30*, 605–615.
46. Du, W.; Peng, Y.M.; Long, S.X.; Nie, H.K.; Sun, C.X.; Ta, Y. Geological characteristics of shale in Wufeng-Longmaxi Formation of Bayu outcrop in Daozhen, northern Guizhou. *Pet. Reserv. Eval. Dev.* **2022**, *12*, 130–138. [[CrossRef](#)]
47. Lin, F.; Bodnar, R.J.; Becker, S.P. Experimental determination of the Raman CH₄ symmetric stretching (ν_1) band position from 1–650 bar and 0.3–22 °C: Application to fluid inclusion studies. *Geochim. Cosmochim. Acta* **2007**, *71*, 3746–3756. [[CrossRef](#)]
48. Zhang, J.; Qiao, S.; Lu, W.; Hu, Q.; Chen, S.; Liu, Y. An equation for determining methane densities in fluid inclusions with Raman shifts. *J. Geochem. Explor.* **2016**, *171*, 20–28. [[CrossRef](#)]
49. Wu, A.; Cao, J.; Zhang, J. Bedding-parallel calcite veins indicate hydrocarbon–water–rock interactions in the over-mature Longmaxi shales, Sichuan Basin. *Mar. Pet. Geol.* **2021**, *133*, 105303. [[CrossRef](#)]

50. Cobbold, P.R.; Rodrigues, N. Seepage forces, important factors in the formation of horizontal hydraulic fractures and bedding-parallel fibrous veins ('beef' and 'cone-in-cone'). *Geofluids* **2007**, *7*, 313–322. [[CrossRef](#)]
51. Cobbold, P.R.; Zanella, A.; Rodrigues, N.; Løseth, H. Bedding-parallel fibrous veins (beef and cone-in-cone): Worldwide occurrence and possible significance in terms of fluid overpressure, hydrocarbon generation and mineralization. *Mar. Pet. Geol.* **2013**, *43*, 1–20. [[CrossRef](#)]
52. Goldstein, R.H. *Systematics of Fluid Inclusions in Diagenetic Minerals*; SEPM: Broken Arrow, OK, USA, 1994.
53. Gao, J. Paleo-temperature and pressure and origin of paleo-fluid of fracture veins in the Wufeng-Longmaxi shales of Yudong area. Ph.D. Thesis, China University of Geosciences, Wuhan, China, 2018.
54. Hall, D.L.; Sterner, S.M.; Bodnar, R.J. Freezing point depression of NaCl-KCl-H₂O solutions. *Econ. Geol.* **1988**, *83*, 197–202. [[CrossRef](#)]
55. Xu, Y.D.; Wang, L.; Liu, Z.C.; Shi, L.Y. Characteristics and accumulation stage of fluid inclusions in volcanic reservoirs in Chepaizi area. *Fault Block Oil Gas Field* **2020**, *27*, 545–550.
56. Gao, J.; Zhang, J.K.; He, S.; Zhao, J.X.; He, Z.L.; Wo, Y.J.; Feng, Y.X.; Li, W. Overpressure generation and evolution in Lower Paleozoic gas shales of the Jiaoshiba region, China: Implications for shale gas accumulation. *Mar. Pet. Geol.* **2019**, *102*, 844–859. [[CrossRef](#)]
57. Becker, S.; Eichhubl, P.; Laubach, S.; Reed, R.; Lander, R.; Bodnar, R. A 48 my history of fracture opening, temperature, and fluid pressure: Cretaceous Travis Peak Formation, East Texas basin. *Bulletin* **2010**, *122*, 1081–1093.
58. Fall, A.; Eichhubl, P.; Bodnar, R.J.; Laubach, S.E.; Davis, J.S. Natural hydraulic fracturing of tight-gas sandstone reservoirs, Piceance Basin, Colorado. *Bulletin* **2015**, *127*, 61–75. [[CrossRef](#)]
59. Marchesini, B.; Carminati, E.; Aldega, L.; Mirabella, F.; Petrelli, M.; Caracausi, A.; Barchi, M.R. Chemical interaction driven by deep fluids in the damage zone of a seismogenic carbonate fault. *J. Struct. Geol.* **2022**, *161*, 104668. [[CrossRef](#)]
60. Klyukin, Y.I.; MacInnis, M.S.; Sanchez, P.L.; Bodnar, R.J. Fluid inclusion phase ratios, compositions and densities from ambient temperature to homogenization, based on PVTX properties of H₂O-NaCl. *Earth Sci. Rev.* **2019**, *198*, 102924. [[CrossRef](#)]
61. Song, Y.; Chen, Y.; Wang, M.; Steele-MacInnis, M.; Ni, R.; Zhang, H.; Fan, J.; Ma, X.; Zhou, Z. In-situ cracking of oil into gas in reservoirs identified by fluid inclusion analysis: Theoretical model and case study. *Mar. Pet. Geol.* **2023**, *147*, 105959. [[CrossRef](#)]
62. Liu, B.; Shen, K. *Fluid Inclusion Thermodynamics*; Geological Press: Beijing, China, 1999.
63. Liu, A.; Ou, W.; Huang, H.; Wei, K.; Li, H.; Chen, X. Significance of paleo-fluid in the Ordovician–Silurian detachment zone to the preservation of shale gas in western Hunan–Hubei area. *Nat. Gas Ind. B* **2018**, *5*, 565–574. [[CrossRef](#)]
64. Liu, D.H.; Xiao, X.M.; Tian, H.; Wang, Y.G.; Wang, Z.C.; Min, Y.S. Multiple types of high density methane inclusions and their relationships with exploration and assessment of oil-cracked gas and shale gas discovered in NE Sichuan. *Earth Sci. Front.* **2013**, *20*, 64–71.
65. Gao, J.; He, S.; Yi, J.Z. Discovery of high density methane inclusions in Jiaoshiba shale gas field and its significance. *Oil Gas Geol.* **2015**, *36*, 472–480.
66. Wang, W.; Wang, G.M.; Hu, J.; Zhang, J.; Wang, Z.; Shi, X.M. Characteristics of Fluid Inclusions and Hydrocarbon Charging Periods of Lower Yanchang Formation in Central Ordos Basin, China. *J. Earth Sci. Environ.* **2020**, *42*, 159–171. [[CrossRef](#)]
67. Liu, D.H.; Dai, J.X.; Xiao, X.M. High density methane inclusions in Puguang gasfield: Discovery and a T-P genetic study. *Chin. Sci. Bull.* **2010**, *55*, 359–366. [[CrossRef](#)]
68. Zgoruchenko, V.A.; Zhuravlev, A.M. *Thermophysical Properties of Gaseous and Liquid Methane*; Israel Program for Scientific Translations: USA, 1970.
69. Jinlei, L.I.; Cheng, Y.I.N.; Mingfei, W.A.N.G.; Shasha, Y.A.N.G.; Xiaojing, L.I.U.; Chao, C.H.E.N. Preservation condition differences in Jiaoshiba area, Fuling, Sichuan Basin. *Pet. Geol. Exp.* **2019**, *41*, 341–347.
70. Yan, Z. *Distribution and Control Factors of Oil and Water in East Wing of Putaohua Oilfield*; 2019; pp. 458–462.
71. Wang, J. Study on Diagenetic response process and gas reservoir forming mechanism of marine shale under the typical compressional tectonic environment. Ph.D. Thesis, ChengDu University of Technology, Chengdu, China, 2021.

Disclaimer/Publisher's Note: The statements, opinions and data contained in all publications are solely those of the individual author(s) and contributor(s) and not of MDPI and/or the editor(s). MDPI and/or the editor(s) disclaim responsibility for any injury to people or property resulting from any ideas, methods, instructions or products referred to in the content.